frontiers in Earth Science

ORIGINAL RESEARCH
published: 19 March 2021
doi: 10.3389/feart.2021.639459

A Multidisciplinary Investigation Into the Eruptive Style, Processes, and Duration of a Cascades Back-Arc Tholeiitic Basalt: A Case Study of the Brushy Butte Flow Field, Northern California, United States

Drew T. Downs[1], Duane E. Champion[2], Michael A. Clynne[2] and L. J. Patrick Muffler[2]*

[1]U.S. Geological Survey, Hawaiian Volcano Observatory, Hilo, HI, United States, [2]U.S. Geological Survey, California Volcano Observatory, Menlo Park, CA, United States

OPEN ACCESS

Edited by:
Rosa Anna Corsaro, National Institute of Geophysics and Volcanology, Italy

Reviewed by:
Karoly Németh, Massey University, New Zealand
Daniel Heaton, Oregon State University, Corvallis, United States

***Correspondence:**
Drew T. Downs
ddowns@usgs.gov

Specialty section:
This article was submitted to Volcanology, a section of the journal Frontiers in Earth Science

Received: *09 December 2020*
Accepted: *08 February 2021*
Published: *19 March 2021*

Citation:
Downs DT, Champion DE, Clynne MA and Muffler LJP (2021) A Multidisciplinary Investigation Into the Eruptive Style, Processes, and Duration of a Cascades Back-Arc Tholeiitic Basalt: A Case Study of the Brushy Butte Flow Field, Northern California, United States. Front. Earth Sci. 9:639459. doi: 10.3389/feart.2021.639459

The Cascades back-arc in northern California is dominated by monogenetic tholeiitic basalts that erupted throughout the Pleistocene. Elucidating their eruptive history and processes is important for understanding potential future eruptions here. We focus on the well-exposed monogenetic volcano that emplaced the Brushy Butte flow field, which constructed a ~150 m tall edifice, has flow lobes up to >10 km long, and in total covers ~150 km^2 with an eruptive volume of 3.5 km^3. We use a multidisciplinary approach of field mapping, petrography, geochemistry, paleomagnetism, geochronology, and lidar imagery to unravel the eruptive history and processes that emplaced this flow field. Tholeiitic basalts in northern California have diverse surface morphology and vegetation cover but similar petrographic appearances, which makes them hard to distinguish in the field. Geochemistry and paleomagnetism offer an independent means of distinguishing tholeiitic basalts. Brushy Butte flow field lavas are similar in major-oxide and trace-element abundances but differ from adjacent tholeiitic basalts. This is also apparent in remanent magnetic directions. Additionally, paleomagnetism indicates that the flow field was emplaced during a geologically brief time interval (10–20 years), which ^{36}Cl cosmogenic dating puts at 35.7 ± 1.7 ka. Lidar imagery shows that these flows erupted from at least 28 vents encompassing multiple scoria cones, spatter cones, and craters. Flows can be grouped into four pulses using stratigraphic position and volume. Pulse 1 is the most voluminous, comprising eight eruptions and ~2.3 km^3. Each subsequent pulse started rapidly but decayed quickly, and each successive pulse erupted less lava (i.e., 2.3 km^3 for pulse 1, 0.6 km^3 for pulse 2, 0.3 km^3 for pulse 3, and 0.2 km^3 for pulse 4). Many of these flows host well-established lava channels and levees (with channel breakouts) that lead to lava fans, with some flows hosting lava ponds. Similar flow features from tholeiitic eruptions elsewhere demonstrate that these morphologies generally occur over weeks, months, or longer (e.g., Pu‘u ‘Ō‘ō eruption at Kīlauea, Hawai‘i). This multidisciplinary study shows the range of eruptive styles and durations of a Cascades

back-arc eruption and illustrates how potential future tholeiitic eruptive activity in the western United States might progress.

Keywords: Cascades volcanic arc, back-arc, tholeiitic basalt, lava flows, flow field

INTRODUCTION

An important objective of investigating active volcanic terrains is to understand hazards posed and how best to mitigate future risks. Geologic aspects necessary to understanding hazards include: 1) nature of vent(s); a single, long-lived vent vs. numerous, diffuse monogenetic vents, 2) eruptive styles that are predominantly effusive, explosive, or both, 3) erupted volumes, 4) geographic distribution of vents and eruptive products, 5) duration of eruptions or eruptive episodes, and 6) recurrence interval between eruptions or eruptive episodes. Satisfactorily investigating these aspects requires a multidisciplinary approach to unravel the geologic framework of a volcano or volcanic field.

The southern part of the Cascades volcanic arc in northern California, United States (**Figures 1A,B**), is a region with abundant vents that have experienced diverse eruptive processes and styles. This part of the Cascades volcanic arc encompasses Mount Shasta, Medicine Lake Volcano, and the Lassen Volcanic Center (**Figure 1B**). The high-standing, morphologically rough appearances of these volcanic regions testify to Late Pleistocene and Holocene eruptions that constructed and modified their edifices. Recognition that these volcanically active areas encompass young lava and pyroclastic flows, and thus pose different potential hazards, has been a motivating factor for geologic investigations that include field mapping, volcanic stratigraphy, petrography, paleomagnetism, geochemistry, and geochronology to elucidate the compositions, styles, durations, and timing of eruptions (e.g., Christiansen et al., 2002; Christiansen et al., 2017; Hildreth, 2007; Clynne and Muffler, 2010, 2017; Donnelly-Nolan, 2010; Muffler and Clynne, 2015; Donnelly-Nolan et al., 2016; Donnelly-Nolan and Grove, 2017).

In northern California, the topographically subdued region east of the calc-alkaline arc front is the back-arc (**Figure 1B**), which is dominated by low-K olivine tholeiitic basalt (also commonly referred to as high-Al olivine tholeiitic basalt) throughout the Pleistocene. These tholeiitic basalts fill valleys and surround many of the older calc-alkaline volcanic edifices (Muffler and Clynne, 2015; Champion et al., 2017; Clynne and Muffler, 2017; Muffler et al., 2017; Downs et al., 2020a). Some of these tholeiitic basalts have rough, primary surface morphologies owing to sparse vegetation in the arid environment, which makes them look youthful (**Figures 2A,C,D**). Miller (1989) used the young appearance of flows to propose that more than a dozen eruptions occurred in the back-arc of northern California during the Holocene. Yet, only a few tholeiitic basalt eruptions in northern California have been studied in detail by field mapping, petrography, geochemistry, and geochronology (e.g., Giant Crater flow field by Baker et al., 1991; Donnelly-Nolan et al., 1991, Hat Creek Basalt by Muffler et al., 1994; Turrin et al., 2007, and Eagle Lake tholeiitic basalts by Clynne et al., 2017), with recent studies currently unraveling the volcanic stratigraphy, compositions, and timing of other eruptions in this region (Champion et al., 2017; Muffler et al., 2017; Downs et al., 2020a). Despite the relatively infrequent eruption of tholeiitic basalts (>20 tholeiitic basalt eruptions from 1800 to 24 ka: Muffler et al., 2017), the back-arc of northern California encompasses young-appearing eruptions throughout the Late Pleistocene and is considered volcanically active. Here, we investigate young-appearing, back-arc tholeiitic basalts of the Brushy Butte flow field (**Figures 1B**, **2A**,**B**).

The Brushy Butte flow field differs from other typical monogenetic tholeiitic basalts in northern California in that its eruptions constructed a relatively high-standing edifice ~150 m tall from at least 29 vents and (or) lava flows that we have grouped into four pulses. The distinct edifice and young appearance of the flow field prompted reconnaissance fieldwork to: 1) establish the veracity of the existing mapping (Peterson and Martin, 1980), 2) determine the age of what was considered a 'very low threat volcano' by the California Volcano Observatory (Miller, 1989; Ewert et al., 2018), and 3) determine the range of geochemical compositions of lavas from the flow field. This resulted in a multidisciplinary approach (see **Supplementary Table S1** in the **Supplementary Material** for a list of samples and associated analyses undertaken) to resolve the eruptive styles, compositions, duration, and timing of emplacement of the Brushy Butte flow field and put this flow field into context with the surrounding volcanic terrain.

Our data and interpretations demonstrate that the edifice of the Brushy Butte flow field was constructed by a vent complex erupting flows during the Late Pleistocene. The tholeiitic basalts erupted have similar outcrop, hand specimen, and petrographic characteristics that are nearly identical to the characteristics of most surrounding tholeiitic basalts, but each of these basalts has a unique geochemical composition. As such, the Brushy Butte lavas are internally similar but geochemically distinct from surrounding, commonly young-appearing tholeiitic basalts (e.g., the Late Pleistocene flow field of Giant Crater).

The Brushy Butte flow field was emplaced over a geologically short time interval (years to decades) based on similarities in mean remanent directions of magnetization, with individual flows that make up the flow field erupting over weeks to months based on the development of volcanic features that form during long-duration extrusive events (e.g., well-established channels, levees, and lava ponds). Our research on the young-appearing eruptions of the Brushy Butte flow field demonstrates how future tholeiitic basalt eruptions in this region might progress.

Geologic Background

The Cascades volcanic arc is the surface manifestation of volcanism on continental crust of the North American plate

due to subduction of the Explorer, Juan de Fuca, and Gorda oceanic plates along the Cascadia subduction zone (**Figure 1A**). Volcanism is most apparent as the remarkable, high-standing edifices of calc-alkaline stratovolcanoes (e.g., Mount Rainier, Mount Hood, Mount Shasta, etc.) that make up much of the surface expression of the Cascades volcanic arc (Hildreth, 2007). In the southern part of the Cascades volcanic arc in northern California, Quaternary volcanism is concentrated at the long-lived volcanic centers of the Mount Shasta stratovolcano and around the volcanic fields of the Lassen Volcanic Center and Medicine Lake Volcano (**Figure 1B**). Radiocarbon and radiometric dating confirm the presence of Holocene eruptions from Mount Shasta, Medicine Lake Volcano, and the Lassen Volcanic Center (Christiansen et al., 2017; Clynne

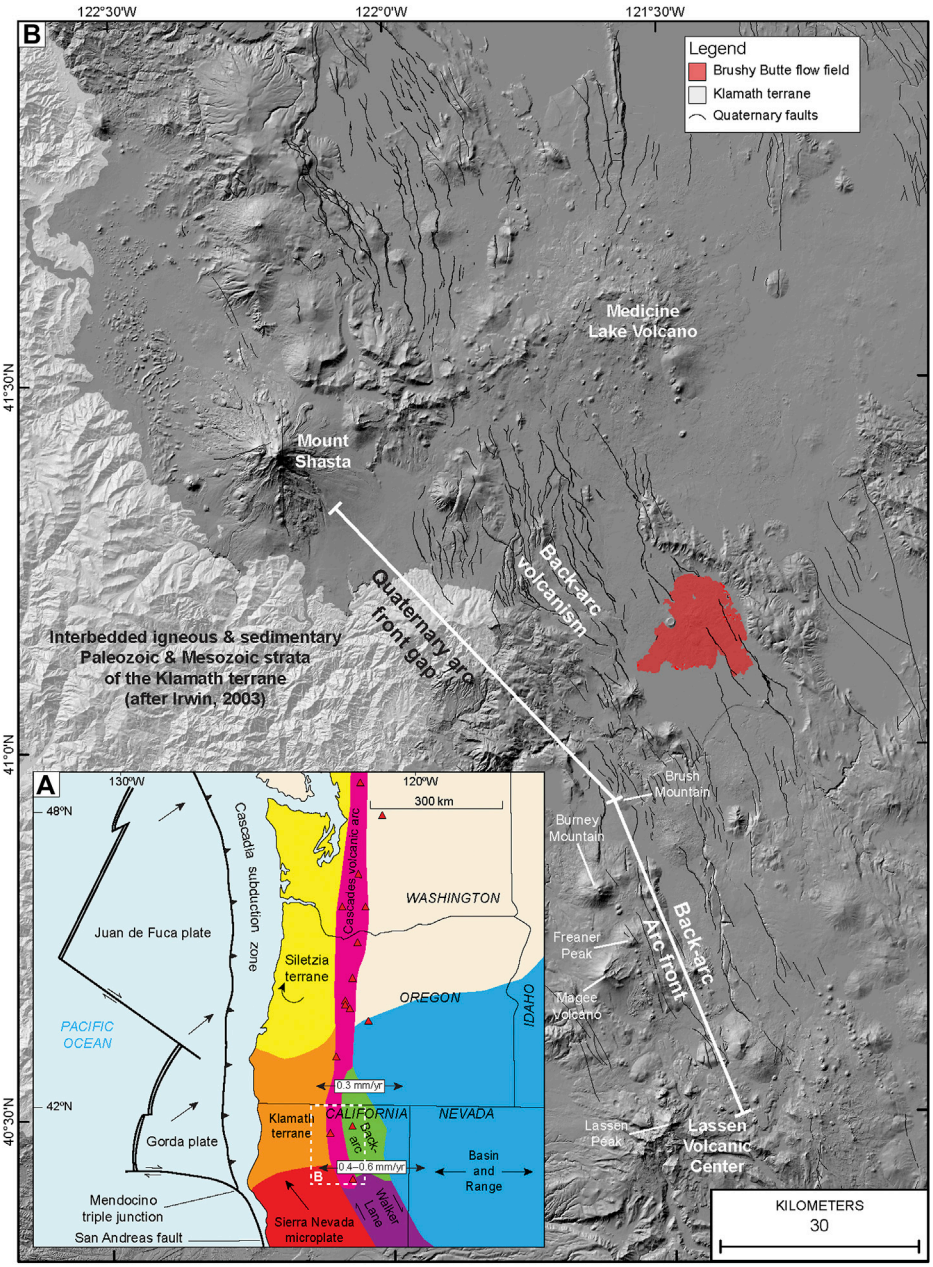

FIGURE 1 | (A) Tectonic setting of western North America, with red triangles denoting major volcanic centers. Dashed box is location shown in **(B)**. Arrows show directions of motion for parts of North America and subducting oceanic plates. **(B)** Shaded-relief terrain model (12 m-resolution TanDEM-X digital elevation model from the German Aerospace Center, 2017) of the southernmost part of the Cascades volcanic arc showing the long-lived, active volcanic centers of Mount Shasta, Medicine Lake Volcano, and the Lassen Volcanic Center. The Brushy Butte flow field in the back-arc is shown in red, as are the abundant back-arc north-northwest-striking normal faults (from the U.S. Geological Survey Quaternary fault and fold database of Machette et al., 2004). Mesozoic sedimentary and igneous rocks of the Klamath terrane are present west of Quaternary volcanic rocks (after Irwin, 2003).

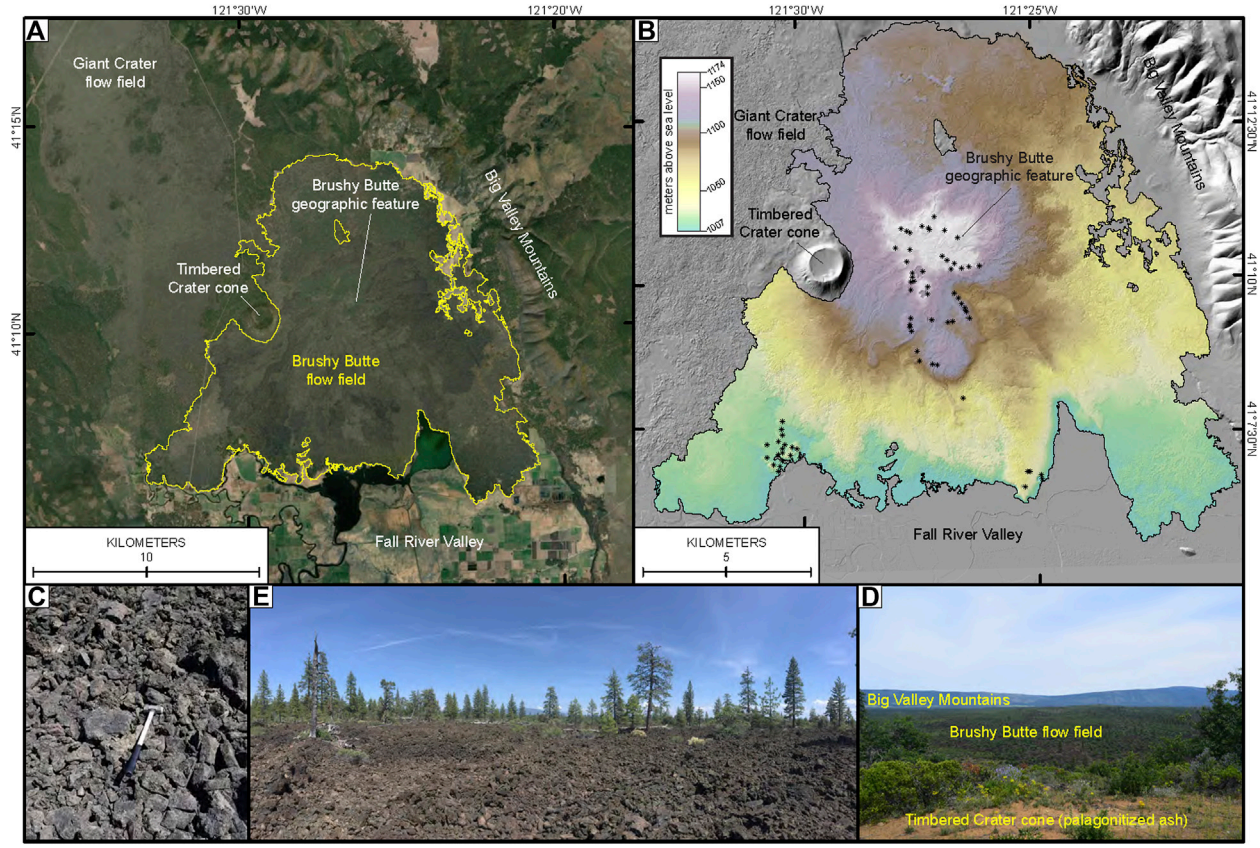

FIGURE 2 | (A) Satellite imagery showing the youthful appearance of the Brushy Butte (with the Brushy Butte geographic feature noted) and Giant Crater flow fields. **(B)** 1 m-resolution lidar derived hillshade and colored DEM showing the topographic roughness of the Brushy Butte flow field. * symbols denote the locations of vents, such as scoria cones, spatter cones, and craters, of which multiple effusion points are common for tholeiitic basalt eruptions. **(C)** View of sparsely vegetated, young-looking slabby pāhoehoe lava flow from the Brushy Butte flow field. The horizontal flat lava plates are ideal for ^{36}Cl cosmogenic surface-exposure dating. Photograph was taken at 41.15528 N, 121.51449 W. **(D)** View looking east into the morphologically rough, sparsely vegetated surface of the Brushy Butte flow field. Photograph was taken at 41.14666 N, 121.50854 W. **(E)** View looking east from the top of the Timbered Crater cone (reddish-tan palagonitized ash in the foreground) looking at the low-lying Brushy Butte flow field and the high-standing Big Valley Mountains. Photograph was taken at 41.17164 N, 121.48444 W.

et al., 2017; Donnelly-Nolan and Grove, 2017), but the only eruption documented first-hand was at Lassen Peak in 1914–1917 (Christiansen et al., 2002; Clynne and Muffler, 2010, 2017; Muffler and Clynne, 2015).

The southernmost locus of arc-related eruptions during the Quaternary is near Lassen Peak (in the Lassen Volcanic Center). The axis of the arc extends between Mount Shasta and Medicine Lake Volcano farther north into Oregon, Washington, and southern Canada (**Figure 1A**). For ~50 km north of Lassen Peak, the arc front is expressed as prominent high-standing Middle and Late Pleistocene calc-alkaline (dominantly andesite and dacite) edifices, such as Magee Volcano, Freaner Peak, Burney Mountain, and Brush Mountain (**Figure 1B**; Muffler and Clynne, 2015; Clynne and Muffler, 2017; Downs et al., 2020b). North of Brush Mountain for ~70 km, Pleistocene calc-alkaline volcanic edifices are absent along the arc front. Situated east of the calc-alkaline arc front are relatively thin (typically 10–15 m thick, but thicker where they fill valleys), voluminous and laterally extensive, tholeiitic basalt flows that erupted throughout the Pleistocene (Champion et al., 2017; Muffler et al., 2017; Downs et al., 2020a). These tholeiitic basalts are eruptive products of the back-arc and overlie and surround older Quaternary and Neogene calc-alkaline volcanic edifices that are earlier expressions of the eastward-migrating Cascades volcanic arc (Guffanti et al., 1990; Borg et al., 2002).

Older tholeiitic basalts in the back-arc (predominantly those of the Early and Middle Pleistocene) tend to be deeply weathered, densely vegetated, commonly expressed as rounded boulders protruding from well-developed soils (sometimes >10 m thick). Late Pleistocene tholeiitic basalts are more conspicuous owing to the arid environment of northeastern California, with sparse vegetation, soil development, and erosion (**Figure 2A**). As such, most of the surface morphologies of Late Pleistocene basalt flows in the back-arc are well preserved, lending these tholeiitic basalts a young, rough appearance (**Figures 2C–E**). This appearance resulted in most of them being assigned to the Holocene (cf., Peterson and Martin, 1980; Miller, 1989; Grose, 1999). However, several of these back-arc tholeiitic basalts now have isotopic ages showing them to be older than Holocene (Giant Crater flow field in Donnelly-Nolan, 2010, Hat Creek

Basalt in Turrin et al., 2007, and Eagle Lake tholeiitic basalts in Clynne et al., 2017).

Mapping of the Brushy Butte flow field and surrounding region was first undertaken by Peterson and Martin (1980) as a U.S. Geological Survey Wilderness Study Area, with their mapped units mostly incorporated into later mapping undertaken farther east by Grose (1999). The Brushy Butte flow field was assigned a Holocene age based on the relatively rough, sparsely vegetated flow surfaces present throughout much of its extent (**Figures 2C–E**; Peterson and Martin, 1980; Miller, 1989). This Holocene age assignment resulted in Miller (1989) designating the Brushy Butte flow field as having the potential to cause future ash and lava hazards equivalent to the largest basaltic flow and airfall tephra hazards (i.e., up to 10 km from vent) in the northern California back-arc. As a result, the Brushy Butte flow field was considered a 'very low threat volcano' in need of monitoring (Ewert et al., 2005; Ewert, 2007); however, it has recently been taken off the threat list as a result of its stratigraphic position negating the Holocene eruption age (Ewert et al., 2018) and the recognition that northern California back-arc tholeiitic basaltic eruptions are indicative of monogenetic volcanism (e.g., Wood, 1979; Németh and Kereszturi, 2015). Despite being removed from the threat list, none of the aforementioned investigations dealt with the eruptive styles, compositions, or ages of the Brushy Butte flow field or surrounding tholeiitic basalts.

METHODS AND RESULTS

Geologic Mapping

During this study, tholeiitic basalt flows were mapped in the field using petrographic characteristics in an attempt to identify contacts and stratigraphic superposition. However, petrographic similarities and the unreliable nature of using visual observations based on vegetation cover and type indicated that a multidisciplinary approach for discriminating between flows would be required. Geochemical and paleomagnetic data provide two independent means of discriminating between tholeiitic basalts in the back-arc of northern California (e.g., Champion et al., 2017; Muffler et al., 2017; Downs et al., 2020a).

Our mapping was supported by 1 m-resolution lidar (available from the U.S. Geological Survey 3D Elevation Program: https://www.usgs.gov/core-science-systems/ngp/3dep) to help identify contacts between flow units and locate potential sampling sites. Processing of lidar data strips away vegetation cover to show the underlying terrain, making the surface morphology of flows and other volcanic landforms more prominent. Flows from the Early and Middle Pleistocene show smoother surface morphologies as a result of extensive soil development and erosion. Late Pleistocene flows, while moderately to sparsely vegetated along internal flow contacts, faults, and in more scoria-rich deposits, still have relatively intact primary surface morphologies (**Figures 2C,D**). In particular, surface features such as well-established channels and levees, channel breakouts, lava ponds, inflated pāhoehoe surfaces, scoria cones, spatter cones, and craters are evident throughout the Brushy Butte flow field (**Figure 2B**). This vastly aids in understanding the emplacement history of these flows when integrated with other datasets (e.g., geochemistry, paleomagnetism, and geochronology). Additionally, the lidar imagery provides a vital window into parts of the flow field that cannot be directly sampled because they lie within Pit River tribal lands, Ahjumawi Lava Springs State Park, private property, or in terrain that is difficult to access. Using the lidar imagery, we can interpret stratigraphic context, flow morphologies, and make important inferences as to eruptive styles and emplacement processes. The integration of all of these data has resulted in a detailed geologic map of the Brushy Butte flow field and the flows and other geologic units with which it is in contact (**Figure 3** and see **Supplementary Figure S1** in the **Supplementary Material** for a high-resolution version of the geologic map).

Geochemistry and Petrography

Geochemical data were helpful for distinguishing various flows and identifying the locations of contacts throughout this region. A total of 82 lava samples from the Brushy Butte region were collected for major-oxide and trace-element analyses by wavelength-dispersive X-ray fluorescence (WD-XRF) spectrometry (after Johnson et al., 1999; see the **Supplementary Material** for a description of the methods). Forty-three samples are from the Brushy Butte flow field, whereas the other 39 analyses are from surrounding flows and help distinguish them from the Brushy Butte lavas (see **Supplementary Table S2** in the **Supplementary Material** for all analyses). Additionally, six samples from various lobes of the Brushy Butte flow field were analyzed by laser ablation-inductively coupled plasma-mass spectrometry (LA-ICP-MS) as a secondary check on internal variations of different eruptive pulses of the flow field (**Table 1**; see the **Supplementary Material** for methods).

All but one of the tholeiitic basalt flows displayed on **Figure 3** have very similar petrographic characteristics: diktytaxitic groundmass hosting 1–3% olivine phenocrysts of 1–2 mm diameter and rare (<<1%) plagioclase phenocrysts. The exception is the Thousand Springs flow, which has common (1–2%, to 1–2 mm) plagioclase phenocrysts that have resorbed cores with sieve textures and overgrowth rims. This flow also has a distinctive geochemistry, with a large range for many major-oxide and trace-element abundances. For example, the Thousand Springs composition ranges from 48.77 to 52.52 wt% SiO_2 and 0.24 to 1.01 wt% K_2O compared to 47.41 to 48.04 wt% SiO_2 and 0.09 to 0.15 wt% K_2O for the Brushy Butte flow field.

Both major oxides and trace elements are useful for distinguishing the other petrographically similar tholeiitic basalts as a result of magma chemistry being controlled by the degree, depth, and mineralogy of the metasomatized mantle lithosphere undergoing partial melting (e.g., Champion et al., 2017; Muffler et al., 2017; Downs et al., 2020a). Some of the major-oxide and trace-element abundances overlap, but significant differences allow distinct flows to be defined. **Figure 4** shows a suite of plots used to distinguish the

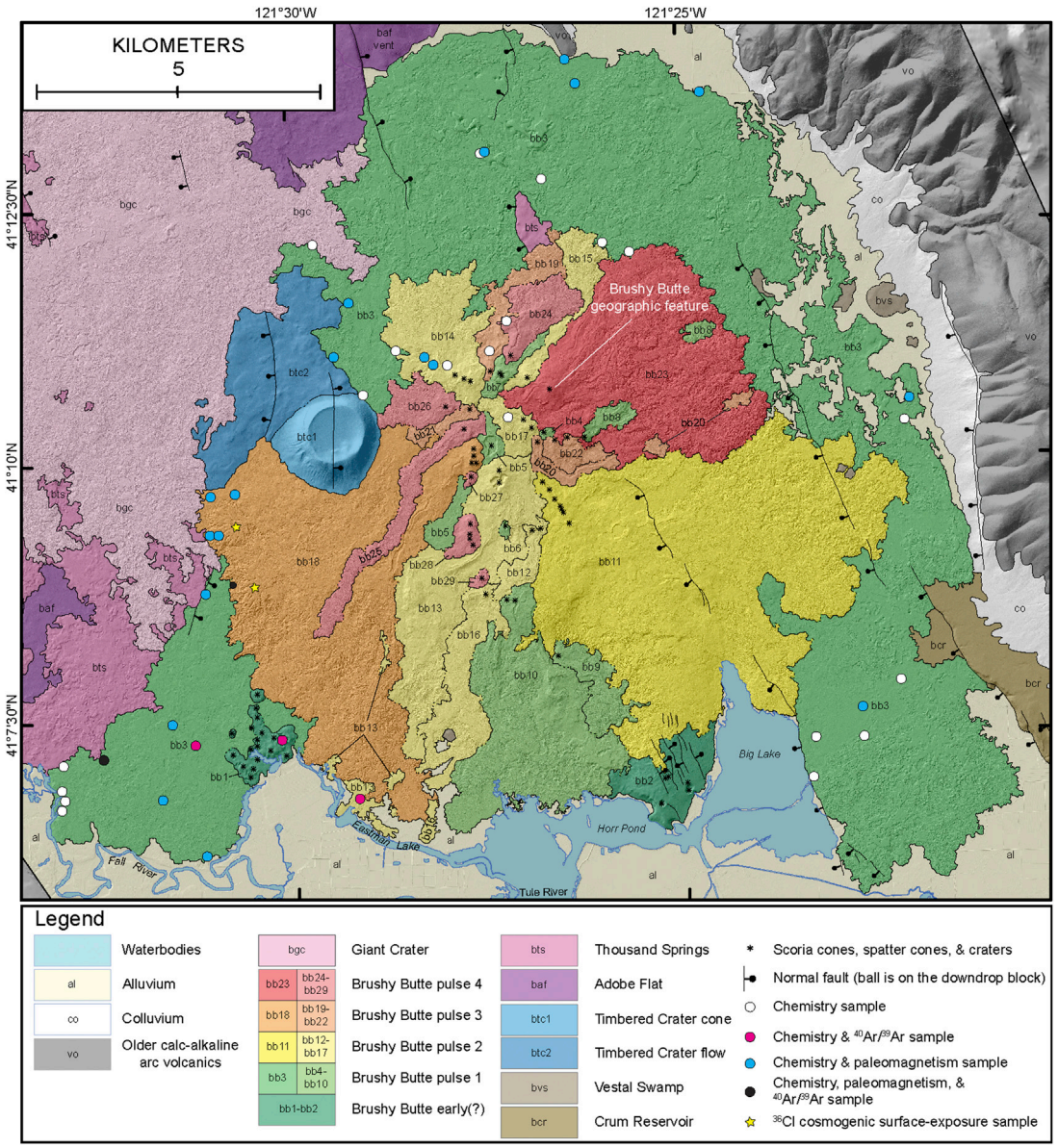

FIGURE 3 | Geologic map of the Brushy Butte flow field (with the Brushy Butte geographic feature noted), surrounding tholeiitic basalts, alluvium, colluvium, and older calc-alkaline volcanic rocks. Monogenetic tholeiitic basalt flows erupted during the Pleistocene are arranged in stratigraphic order from youngest (Giant Crater) to oldest (Crum Reservoir). The Brushy Butte flow field is divided into units bb1–bb29, which are placed within the early (?) Brushy Butte (bb1–bb2), with the remaining units making up pulses 1–4. Pulses 1–4 are divided into their initially erupted flows (darker color in the legend) followed by the rest of the eruptions of that pulse (lighter color of the same pulse in the legend).

different tholeiitic basalt flows displayed on **Figure 3**. The Brushy Butte flow field tends to have relatively low, but slightly overlapping, abundances of TiO_2 (0.69–0.89 wt%) with surrounding tholeiitic basalts at their given MgO abundances (**Figure 4**). As a result, the Brushy Butte geochemical field (gray area in **Figure 4**) generally plots in a distinct position for TiO_2 versus other major-oxide and trace-elements. A distinct field is also noticeable for trace-element plots, particularly those using Zr, to discriminate the Brushy Butte geochemical field from surrounding tholeiitic basalts.

The Giant Crater flow field (Group 5 as mapped by Donnelly-Nolan et al., 1991) directly contacts the west side of the Brushy Butte flow field and closely resembles these lavas (**Figures 2A,B**). Our whole-rock analyses from Giant Crater overlap the limited range of values for Group 5 presented in Baker et al. (1991) and Donnelly-Nolan et al. (1991). Brushy Butte and Giant Crater major-oxide abundances plot within close proximity and commonly overlap, although there are observable differences in FeO*, MnO, CaO, and K_2O. On the other hand, trace-element values of Brushy Butte and Giant Crater rarely

TABLE 1 | Trace-element geochemical analyses of the Brushy Butte flow field.

Sample number	B17DD077	B18DD132	B19DD166	B19DD173	B18DD147	B18DD143	Standard Deviations
Pulse	Pulse 1	Pulse 1	Pulse 1	Pulse 1	Pulse 2	Pulse 3	
Unit	bb3	bb3	bb3	bb3	bb14	bb18	
Latitude	41.12149	41.22685	41.17218	41.12085	41.18210	41.14699	
Longitude	−121.52218	−121.43839	−121.36870	−121.37871	−121.46946	−121.51300	
Ag	0.03	0.03	0.04	0.04	0.04	0.03	0.00
As	0.16	0.11	0.22	0.18	0.14	0.12	0.04
Ba	65.48	72.27	74.21	68.78	76.47	68.72	3.71
Bi	0.01	0.01	0.00	0.01	0.01	0.00	0.00
Cd	0.06	0.06	0.06	0.06	0.06	0.07	0.00
Cr	207.60	207.78	212.71	205.62	204.82	212.63	3.11
Cs	0.05	0.03	0.03	0.03	0.04	0.04	0.01
Cu	103.69	97.64	103.60	130.62	101.09	111.78	10.95
Ga	14.91	14.93	15.05	15.39	15.41	15.15	0.20
Hf	1.14	1.14	1.18	1.26	1.20	1.28	0.06
Mo	0.23	0.29	0.18	0.17	0.20	0.19	0.04
Nb	0.75	0.78	0.86	0.74	0.87	0.77	0.05
Ni	179.26	181.34	163.91	143.86	150.75	161.01	13.67
Pb	0.69	0.64	0.65	0.67	0.63	0.67	0.02
Rb	1.13	0.87	0.78	0.99	1.13	1.00	0.13
Sb	0.02	0.02	0.02	0.03	0.02	0.03	0.00
Sc	37.22	37.29	38.94	41.63	39.14	38.63	1.47
Sn	0.53	0.48	0.55	0.59	0.49	0.53	0.03
Sr	226.13	222.47	224.32	219.00	223.19	220.04	2.42
Ta	0.11	0.09	0.11	0.09	0.09	0.09	0.01
Th	0.15	0.17	0.18	0.14	0.16	0.16	0.01
Tl	0.01	0.01	0.01	0.02	0.01	0.01	0.00
U	0.05	0.05	0.05	0.03	0.05	0.04	0.01
V	203.89	201.19	210.57	219.49	229.35	209.11	9.57
Y	20.99	20.81	22.12	23.68	22.13	22.39	0.95
Zn	66.13	65.46	66.28	68.27	66.31	68.85	1.23
Zr	43.13	41.86	45.86	48.88	44.07	45.80	2.26
La	2.18	2.28	2.39	2.34	2.28	2.34	0.06
Ce	6.29	6.28	6.43	6.80	6.64	6.65	0.19
Pr	1.09	1.10	1.12	1.18	1.11	1.13	0.03
Nd	5.84	5.90	6.07	6.62	6.14	6.29	0.26
Sm	2.02	2.04	2.07	2.26	2.02	2.16	0.09
Eu	0.89	0.88	0.90	0.95	0.87	0.94	0.03
Gd	2.62	2.63	2.80	2.99	2.70	2.83	0.13
Tb	0.51	0.49	0.52	0.57	0.53	0.55	0.03
Dy	3.34	3.39	3.58	3.82	3.61	3.61	0.16
Ho	0.78	0.75	0.82	0.87	0.80	0.81	0.04
Er	2.31	2.27	2.42	2.56	2.44	2.46	0.09
Tm	0.36	0.35	0.37	0.40	0.38	0.38	0.02
Yb	2.34	2.34	2.47	2.62	2.54	2.48	0.10
Lu	0.36	0.35	0.38	0.39	0.38	0.38	0.01

Trace-element (as ppm) analysis were performed by laser ablation-inductively coupled plasma-mass spectrometry (LA-ICP-MS) at the Hamilton Analytical Lab at Hamilton College, Clinton, NY, United States (methods of Conrey et al., 2019). Latitude and longitude are reported in WGS84. See the ***Supplementary Material*** *for details on the method.*

overlap, with characteristic differences in Sc, Cr, Ni, Sr, Rb, and in particular Zr (**Figure 4**; see **Supplementary Table S2** in the **Supplementary Material**).

The high-standing (~150 m tall) interior of the Brushy Butte flow field consists of many flows and vent systems that we have mapped as units bb1–bb29 and divided into four eruptive pulses (**Figure 3**). Geochemical analyses from the flow field shows that the mapped eruptive units, and eruptive pulses, are internally consistent geochemically. Brushy Butte early (?) and pulse 4 have only one analysis each, but both analyses fall within the range of Brushy Butte major-oxide and trace-element abundances from the other pulses (**Figure 4**). Available geochemical evidence is consistent with lavas from the Brushy Butte flow field being distinct from surrounding tholeiitic basalts with which they are in contact.

As a further evaluation of the internal consistency of the Brushy Butte flow field, six samples were analyzed by LA-ICP-MS (**Table 1**). These samples include four from pulse 1 (unit bb3), one from pulse 2 (unit bb14), and one from pulse 3 (unit bb18). The six samples analyzed by LA-ICP-MS all have small

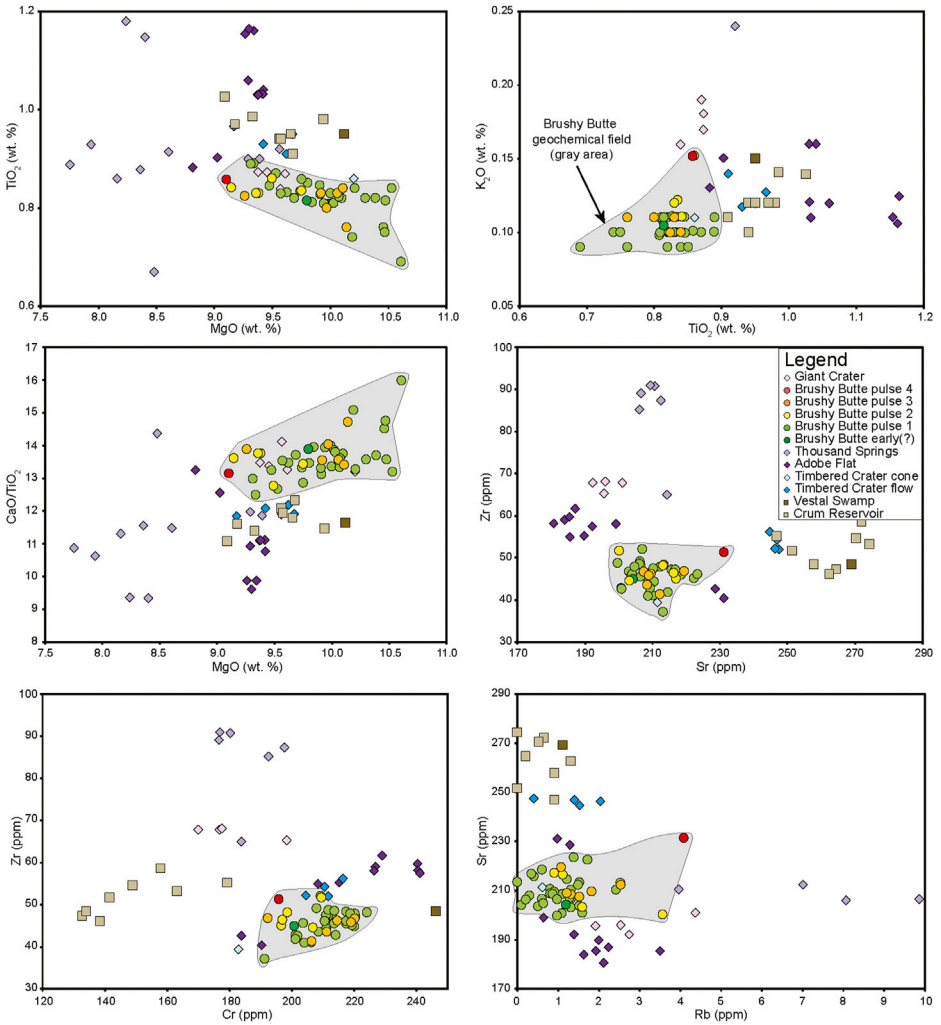

FIGURE 4 | Bivariate plots showing the whole-rock geochemical differences between the Brushy Butte flow field (circles surrounded by the solid black line) and surrounding tholeiitic basalts. The entire Brushy Butte geochemical field is shaded gray. See **Supplementary Table S2** in the **Supplementary Material** for all of the geochemical analyses from the Brushy Butte flow field and the surrounding tholeiitic basalts.

standard deviations and fall within analytical uncertainty of each other by this method (Conrey et al., 2019). For example, Zr abundances for these tholeiitic basalts are generally distinct and these values range from 41.86 to 48.88 ppm (standard deviation of 2.26). The combination of the whole-rock WD-XRF and LA-ICP-MS analyses supports the interpretation that lavas from the Brushy Butte flow field are magmatically identical to one another.

Paleomagnetism

Paleomagnetic data provide an additional and independent test for distinguishing visually and petrographically similar flows and locating contacts. This is a result of the brief timeframe during which the Earth's magnetic field is stationary (4–5° per century of wander; Champion and Shoemaker, 1977).

Paleomagnetic samples were collected, processed, and interpreted using the standard protocols outlined in McElhinny (1973), with a total of 28 sites from five tholeiitic basalt flows. Twenty of these sites were drilled in the Brushy Butte flow field, whereas the remaining eight sites were drilled in surrounding flows to aid in distinguishing them from the Brushy Butte flow field and each other (**Table 2**; see the **Supplementary Material** for methods). The Giant Crater flow field was not drilled for paleomagnetism as part of this study, as this flow field has been well characterized with Champion and Donnelly-Nolan (1994) presenting data from 58 drill sites.

Figure 5A shows the range of mean remanent directions of magnetization for the Brushy Butte flow field and immediately adjacent tholeiitic basalts. Average inclination and declination values for the Brushy Butte flow field are 60.4° and 357.1° (95% confidence level; α95 = 0.8°), respectively. The most visually and morphologically similar basalt in contact with the Brushy Butte flow field is Group 5 of the Giant Crater flow field, for which four drilled sites give average inclination and declination values of

TABLE 2 | Paleomagnetic analyses of the Brushy Butte flow field and surrounding tholeiitic basalts.

Unit / Sample Number	Latitude	Longitude	N/No	Exp.	I	D	α95	k	R	Platitude	Plongitude
Brushy Butte flow field											
B17DD086	41.120	−121.540	8/8	Li	61.7	354.7	1.4	1473	7.99520	85.7	174.3
B17DD096	41.107	−121.520	9/9	Li	61.2	0.1	1.6	1039	8.99230	88.8	242.0
B18DD099	41.113	−121.527	7/8	Li	61.9	358.6	1.3	2049	6.99707	87.7	211.3
B18DD110	41.193	−121.486	7/8	Li	60.9	0.9	1.9	994	6.99396	89.0	280.7
B18DD122	41.176	−121.369	7/8	Li	61.1	348.6	2.1	843	6.99289	81.4	159.2
B18DD151	41.222	−121.457	8/9	Li	61.9	356.0	2.1	690	7.98986	86.5	182.6
B18DD132	41.226	−121.437	8/8	Li	61.2	356.9	1.0	2992	7.99766	87.5	173.1
B18DD152	41.232	−121.439	8/8	Mx	59.9	357.3	2.1	772	7.99090	87.9	137.0
B18DD124	41.147	−121.518	8/8	Li	60.2	357.2	2.6	474	7.98523	87.9	148.0
B18DD150	41.184	−121.490	8/8	Li	63.0	2.9	1.6	1177	7.99405	86.1	271.3
B18DD149	41.126	−121.525	12/12	20	59.4	355.6	1.1	1682	10.99346	86.5	134.6
3B698	41.126	−121.378	11/12	30	59.1	355.1	1.1	1758	10.99431	86.1	131.7
B18DD123	41.226	−121.408	11/12	20	60.2	357.3	1.0	2051	10.99512	88.0	146.6
Pulse 1 average	**41.140**	**−121.470**	**13/13**		**60.9**	**357.0**	**1.0**	**1632**	**12.99265**	**87.6**	**169.3**
B18DD147	41.184	−121.472	6/8	Li	62.0	0.8	1.6	1836	5.99728	87.8	253.4
B18DD148	41.185	−121.477	8/8	Li	59.8	357.4	1.0	3048	7.99770	87.9	133.9
Pulse 2 average	**41.184**	**−121.474**	**2/2**		**60.9**	**359.0**	**6.0**	**1735**	**1.99942**	**89.0**	**195.6**
B18DD127	41.155	−121.515	8/8	Li	58.6	357.4	2.1	705	7.99008	87.3	107.1
B18DD143	41.147	−121.512	8/8	Li	59.6	354.6	3.3	279	7.97487	85.9	139.7
B18DD129	41.162	−121.511	7/7	Li	59.6	359.2	1.5	1700	6.99647	89.0	96.9
B18DD105	41.155	−121.517	12/12	10	57.9	354.6	1.4	971	11.98867	85.1	118.2
B18DD106	41.162	−121.517	11/12	10+	58.1	358.4	0.7	4776	10.99791	87.3	86.2
Pulse 3 average	**41.156**	**−121.515**	**5/5**		**58.8**	**356.8**	**1.3**	**3491**	**4.99885**	**87.1**	**115.3**
Brushy Butte average (all analyses)	**41.140**	**−121.490**	**20/20**		**60.4**	**357.1**	**0.8**	**1578**	**19.98796**	**87.9**	**154.2**
Thousand Springs flow											
B17DD079	41.209	−121.556	8/8	Li	44.4	6.4	1.9	896	7.99220	74.0	37.2
B17DD081	41.129	−121.538	7/8	Mx	44.0	1.2	3.6	324	6.98150	74.6	54.4
B18DD101	41.145	−121.521	5/9	Li	42.8	2.5	1.7	2041	4.99804	73.6	50.6
B18DD104	41.148	−121.524	8/8	Li	43.1	2.2	3.0	343	7.97958	73.8	51.2
Average	**41.160**	**−121.530**	**4/4**		**43.6**	**3.1**	**2.1**	**2006**	**3.99985**	**74.1**	**48.3**
Adobe Flat flow											
B18DD118	41.230	−121.483	8/8	Li	54.5	26.2	2.2	621	7.98874	68.6	336.9
B18DD116	41.217	−121.500	6/8	Li	55.9	22.1	3.2	438	5.98859	72.2	336.7
Average	**41.220**	**−121.490**	**2/2**		**55.2**	**24.2**	**5.9**	**1767**	**1.99943**	**70.4**	**336.8**
Timbered Crater flow											
B17DD080	41.190	−121.499	6/8	Li	71.2	42.8	3.9	300	5.98332	58.8	285.9
Crum Reservoir flow											
B18DD141	41.087	−121.315	8/8	Mx	−37.0	211.2	2.0	792	7.99120	−56.6	176.9

N/No, number of cores used compared with the number originally collected at the site; Exp., nature of site demagnetization analysis; Li, indicates that a vector component lines analysis was used, and Mx, indicates that a mixture of lines and planes was used to define the mean remanent direction; I, remanent inclination in degrees; D, remanent declination in degrees; α95, radius of the 95% confidence limit about the mean direction; k, estimate of the Fisher precision parameter; R, length of the resultant vector; Platitude and Plongitude–location in degrees north and east of virtual geomagnetic pole (VGP) calculated from the mean direction of the site. See the ***Supplementary Material*** *for details on the method.*

59.1° and 18.6° (α95 = 1.4°), respectively (Champion and Donnelly-Nolan, 1994). The inclinations of these two tholeiitic basalts are within error of each other, but their declinations are distinct. The other surrounding tholeiitic basalts are morphologically more subdued in general and also have inclinations and declinations distinct from those of the Brushy Butte flow field (**Table 2** and **Figure 5A**), with the Thousand Springs flow having mean inclinations and declinations of 43.6° and 3.1° (α95 = 2.1°) and the Adobe Flat flow at 55.2° and 24.2° (α95 = 5.9°), respectively. The Timbered Crater flow records an excursional remanent direction at 71.2° and 42.8° (α95 = 3.9°), whereas the Crum Reservoir flow is reversely magnetized at −37.0° and 211.2° (α95 = 2.0°). Crum Reservoir is not shown on **Figure 5A** because of its reverse polarity.

Geochronology

Previous investigations in this region used soil development and vegetation to assign age constraints for flows (Peterson and Martin, 1980; Miller, 1989). While useful for assigning relative ages in certain parts of the map area on **Figure 3**, this approach has limited value as much of the area has been deforested and replanted or cleared for ranch land, and differences in internal surface flow morphologies promote vegetation growth at a range of rates and plant types. Isotopic dating is preferred for understanding the time intervals between eruptions in a given region, although this also is challenging, given the difficulty in finding groundmass or organic matter suitable to analyze from young tholeiitic basalts. Tholeiitic basalts have low abundances of K (0.09–0.15 wt% K_2O for the Brushy Butte flow field; see

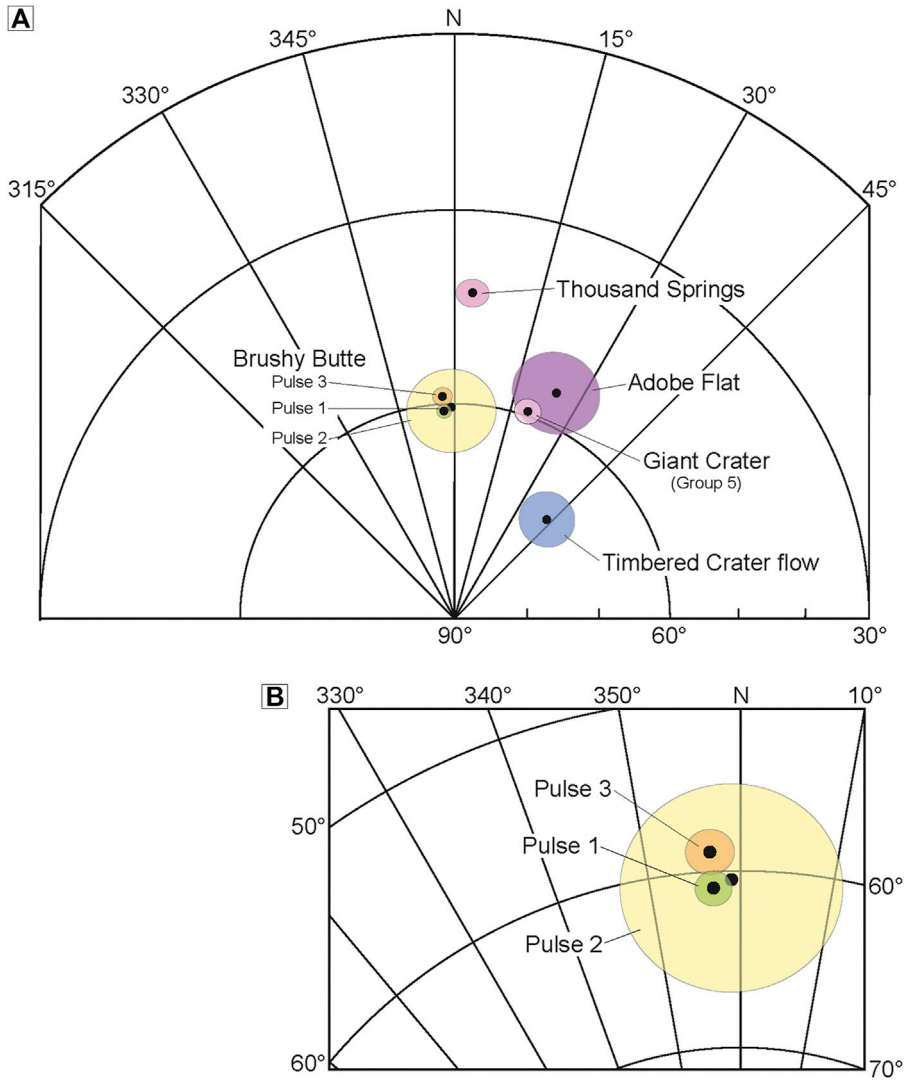

FIGURE 5 | (A) Partial equal-area projection (lower hemisphere) of average mean directions of magnetization and ovals of 95% confidence level (α95) for of pulses 1–3 of the Brushy Butte flow field and surrounding tholeiitic basalts. See **Table 2** for individual sample analysis and for averages from each eruption. **(B)** Close-up view of the average mean directions of magnetization and α95 ovals for pulses 1–3 from the Brushy Butte flow field (see **Table 2** for individual sample analysis and for averages from pulses 1–3).

Supplementary Table S2 in the **Supplementary Material**) and therefore low radiogenic ^{40}Ar, so that Late Pleistocene and Holocene tholeiitic basalts are particularly hard to date by the ^{40}Ar/^{39}Ar method. Analyses of young tholeiitic basalts from northern California by the ^{40}Ar/^{39}Ar method have been successful but only on samples with a nearly perfect coarsely crystalline groundmass lacking vesicles and glass (e.g., Turrin et al., 2007). The young ages of these basalts usually means that there is only minor erosion to expose dense, crystalline groundmass for ^{40}Ar/^{39}Ar dating unless they are cut by major, young faults. Additionally, the ^{14}C method is commonly used for volcanic rocks that erupted <50 ka, but the same arid environment that has allowed remarkable preservation of surface morphologies resulted in the base of the flows not being exposed by erosion. This has made finding organic matter for the ^{14}C method difficult, although not impossible, as Donnelly-Nolan (2010) collected charcoal samples dated at 12.4 ka from the Giant Crater flow field that stratigraphically overlies the Brushy Butte flow field.

A method that has proved useful for providing ages on young flows in arid environments that lack extensive vegetation cover and erosion is the ^{36}Cl cosmogenic surface-exposure dating (e.g., Vazquez and Woolford, 2015; Downs et al., 2018; Downs et al., 2019; Stelten et al., 2018; Stelten et al., 2020; Bromley et al., 2019). We utilized the ^{36}Cl cosmogenic method (see **Supplementary Material** for details on sample collection and analysis) for the Brushy Butte flow field to determine its emplacement age, and we couple this with ^{40}Ar/^{39}Ar ages of surrounding older tholeiitic basalts to better understand the eruptive history of volcanism prior to eruption of the Brushy Butte flow field.

TABLE 3 | $^{40}Ar/^{39}Ar$ ages of the Brushy Butte flow field and surrounding tholeiitic basalts.

			Plateau			Isochron				Total gas
***Lava Flow*/ Sample Number**	**Latitude**	**Longitude**	**% ^{39}Ar (steps, °C)**	**Age ± 1σ (ka)**	**MSWD**	**% ^{39}Ar (steps, °C)**	**Age ± 1σ (ka)**	**MSWD**	**$^{40}Ar/^{39}Ar_i$ ± 2σ**	**Age ± 1σ (ka)**
Brushy Butte flow field										
B17DD077	41.12149	−121.52218	96 (450–1050)	−45 ± 56	0.3	96 (450–1050)	**51 ± 44**	0.2	296.8 ± 6.4	3 ± 66
B17DD086	41.11923	−121.54140	92 (550–1050)	191 ± 56	1.0	100 (450–1150)	**51 ± 17**	1.4	302.4 ± 4.1	332 ± 68
B17DD087	41.12209	−121.50322	100 (450–1150)	−4 ± 52	1.9	35 (850–1150)	**41 ± 27**	1.1	301.0 ± 43.8	68 ± 60
B17DD088	41.11275	−121.48695	100 (450–1150)	**48 ± 52**	1.8	100 (450–1150)	−123 ± 38	1.6	302.7 ± 6.1	80 ± 53
B18DD143	41.14699	−121.51300	83 (450–850)	**165 ± 80**	1.1	83 (450–850)	300 ± 130	1.3	296.1 ± 16.5	411 ± 98
Weighted Mean Age 1				**48 ± 13**	**0.03**					
Weighted Mean Age 2				**52 ± 13**	**0.54**					
Adobe Flat flow										
B18DD114	41.24398	−121.50508	64 (750–1150)	**309 ± 45**	0.5	64 (750–1150)	309 ± 56	0.7	298.5 ± 7.7	621 ± 64
Timbered Crater flow										
B17DD080	41.18938	−121.50034	98 (550–1150)	**571 ± 49**	2.0	98 (550–1150)	428 ± 69	1.0	306.4 ± 8.4	760 ± 59
Vestal Swamp flow										
B18DD140	41.19340	−121.37413	71 (650–1050)	**1053 ± 52**	0.8	71 (650–1050)	964 ± 79	0.3	305.7 ± 20.1	1385 ± 61
Crum Reservoir flow										
B18DD141	41.08481	−121.31781	74 (650–1150)	**1340 ± 59**	0.1	74 (650–1150)	1327 ± 81	0.2	299.3 ± 10.3	1513 ± 60

All samples are groundmass separates. Preferred ages are in bold. Samples were irradiated at the U.S. Geological Survey TRIGA reactor using 9.7946 ± 0.0033 Ma Bodie Hills sanidine as a neutron flux monitor (Fleck et al., 2019). Instrumental mass discrimination was calculated by repeated measurement of atmospheric argon and mass discrimination was calculated assuming atmospheric $^{40}Ar/^{39}Ar = 298.56 \pm 0.31$ (Lee et al., 2006). Ages and errors were calculated using the ^{40}K decay constants of Steiger and Jäger (1977) of $\lambda_{EC} = 0.581 \times 10^{-10}$ yr^{-1}, $\lambda_{\beta^-} = 4.962 \times 10^{-10}$y^{-1}, and $\lambda_{Total} = 5.543 \times 10^{-10}$y^{-1}. MSWD — mean square of weighted deviates. Latitude and longitude are reported in WGS84. Weighted mean age 1 is calculated using samples (B17DD077, B17DD086, B17DD087, and B17DD088, whereas weighted mean age 2 is calculated using all five Brushy Butte flow field ages. See the ***Supplementary Material*** *for details on the method and* ***Supplementary Table S3*** *for the tabulated data and age-spectra from each sample analyzed.*

A few dense, coarse-grained, crystalline samples were identified within the most basal exposed parts of the Brushy Butte flow field, and $^{40}Ar/^{39}Ar$ dating was attempted on five of these (**Table 3**; see the **Supplementary Material** for methods and **Supplementary Table S3** for all tabulated $^{40}Ar/^{39}Ar$ data). These samples yielded ages with large analytical uncertainties (all reported at 1 σ) of 41 ± 27 ka, 48 ± 52 ka, 51 ± 17 ka, 51 ± 44 ka, and 165 ± 80 ka, which span from the Middle Pleistocene to Holocene at 95% confidence levels. Calculating a weighted mean age yields smaller analytical uncertainties of 48 ± 13 ka (using four of five analyses) and 52 ± 13 ka (using all five analyses); however, at the 95% confidence level these still span >25 kyr. The large analytical uncertainties using $^{40}Ar/^{39}Ar$, and a lack of organic matter for ^{14}C dating, prompted the collection of two primary surface rocks (**Figure 2C**) to date by the ^{36}Cl cosmogenic surface-exposure method (**Table 4**; see the **Supplementary Material** for methods and **Supplementary Table S4** for input parameters and output data for calculating the ages). Both surface-exposure ages are nearly identical at 35.4 ± 2.4 ka and 36.0 ± 2.4 ka (analytical uncertainties reported at 1 σ), which yields a weighted mean age of 35.7 ± 1.7 ka. This age overlaps with the $^{40}Ar/^{39}Ar$ ages but yields a significantly smaller analytical uncertainty and clearly places the Brushy Butte flow field within the Late Pleistocene.

Four samples from surrounding tholeiitic basalts in contact with the Brushy Butte flow field were analyzed by the $^{40}Ar/^{39}Ar$ method (**Table 3**). These flows underlie the Brushy Butte flow field and their $^{40}Ar/^{39}Ar$ ages are consistent with their stratigraphic position. The Adobe Flat flow erupted at 309 ± 45 ka, the Timbered Crater flow at 571 ± 49 ka, the Vestal Swamp flow at 1053 ± 52 ka, and the Crum Reservoir flow at 1340 ± 59 ka. Dateable material was not identified from the Thousand Springs flow, which is stratigraphically bracketed by the Brushy Butte flow field at 35.7 ± 1.7 ka and Adobe Flat flow at 309 ± 45 ka. The Timbered Crater cone consists of palagonitized ash that formed during a phreatomagmatic eruption. This cone overlies the Timbered Crater flow, but there is no clear evidence of any eruptive relationship between the cone and flow. A single tholeiitic basalt clast analyzed for geochemistry from the cone does not match the geochemistry of the flow, but it cannot be definitively determined whether this, and similar looking, clasts are juvenile or lithic. The Giant Crater flow field has a ^{14}C age of 12.4 ka (Donnelly-Nolan, 2010), with Ewert et al. (2018) reporting that the Giant Crater flow field overlies the Brushy Butte flow field. This relative age relation is remarkably difficult to see in the field or even using the 1 m-resolution lidar (**Figures 2A,B**). Our age for the Brushy Butte flow field confirms that it is older, and hence underlies, the Giant Crater flow field.

DISCUSSION

The combination of geochemistry and paleomagnetism allows us to reliably map the extent of lavas from the Brushy Butte flow field, and geochronology has allowed them to be placed in their proper volcanic context within the back-arc of northern California (**Figures 1B**, **3**). The 1 m-resolution lidar is a critical tool for interpreting the internal volcanic stratigraphy

TABLE 4 | ^{36}Cl cosmogenic surface-exposure ages from the Brushy Butte flow field.

Sample number	Latitude	Longitude	Elevation (mASL)	Thickness (cm)			Bulk density (g/cm^3)			SF			^{36}Cl/Cl (10^{-15}) ± 1σ	^{36}Cl Atoms g^{-1} (10^5) ± 1σ		^{36}Cl/^{37}Cl ± 1σ			^{36}Cl Ages (ka) ± 1σ		
B18DD126	41.15652	−121.51272	1044	5.5			2.28			1.0			459.6 ± 9.7	3.71 ± 0.08		15.37 ± 0.27			**36.0 ± 2.4**		
B18DD144	41.14666	−121.50854	1046	6			2.01			1.0			412.1 ± 9.8	3.86 ± 0.09		11.10 ± 0.03			**35.4 ± 2.4**		
Sample number	**SiO$_2$**	**TiO$_2$**	**Al$_2$O$_3$**	**Fe$_2$O$_3$**	**MnO**	**MgO**	**CaO**	**Na$_2$O**	**K$_2$O**	**P$_2$O$_5$**	**LOI**	**Cl**	**B**	**Li**	**Sm**	**Gd**	**U**	**Th**			
B18DD105[a]	47.48	0.82	17.35	10.67	0.18	9.93	10.97	2.41	0.10	0.08	0.01	8.6	63	<10	1.8	2.68	<0.05	0.1			
B18DD143[a]	47.52	0.84	17.30	10.64	0.18	9.94	11.03	2.40	0.09	0.07	0.01	15.5	54	<10	2.1	3.06	0.14	0.6			

All ^{36}Cl cosmogenic surface-exposure ages (in bold) were calculated using the CRONUScalc ^{36}Cl Exposure Age Calculator v2.0 (Marrero et al., 2016) and the Lifton/Sato nuclide-dependent, time-dependent scaling model (Lifton et al., 2014). Whole-rock Cl concentrations were measured by isotope dilution at the Purdue Rare Isotope Measurement (PRIME) laboratory at Purdue University. Major-oxides (as wt%) were measured by wavelength-dispersive X-ray fluorescence (WD-XRF) and trace elements (as ppm) were measured by inductively coupled plasma-optical emission spectrometry (ICP–OES) following Taggart (2002). SF is the topographic shielding factor. Latitude and longitude are reported in WGS84 and elevations are in meters above sea level (mASL).

*[a]Due to secondary minerals filling vesicles of surface samples B18DD126 and B18DD144, the ages for these were calculated using the whole-rock compositions of dense, vesicle-free proximal samples B18DD105 and B18DD143, respectively. See the **Supplementary Material** for details on the method and **Supplementary Table S4** for the input parameters used to calculate the ages for sample analyzed.*

of the flow field, so that eruptive styles and emplacement processes can be interpreted. Using the 1 m-resolution lidar, we define 29 vents and (or) flows associated with eruption of the Brushy Butte flow field, which we label as units bb1–bb29 on **Figure 3**. This extends considerably the 12 eruptions Peterson and Martin (1980) proposed for the interior of the flow field. The most extensive and voluminous Brushy Butte flow (unit bb3 on **Figure 3**) was mapped as unrelated to the flow field by Peterson and Martin (1980), who named it the Little Hot Springs Valley flow of the regional Modoc Basalt (unit mlhs on their map).

The eruptions that constructed the Brushy Butte flow field produced 26 flows and at least 28 vent areas (totalling 29 combined vents and [or] flows), including several scoria cones, spatter cones, and craters (**Figure 3** and **Table 5**). These vents and flows built an edifice ~150 m tall, and some of the flows reach >10 km from their vents. We infer the underlying topography to have been relatively flat and level (similar to the present-day Fall River Valley farther south), as the early erupted pāhoehoe flows (primarily unit bb3 on **Figure 3**) are distributed at mostly equal distances in a radial arrangement around the main central vent area. Later formed vents erupted predominantly ʻaʻā flows (**Figures 2C,D**) in the interior of the flow field; the ʻaʻā did not flow as far and built most of the interior edifice of the flow field (e.g., Walker, 1973). **Table 5** summarizes the characteristics of each Brushy Butte eruptive unit, with areal extents, flow lengths, and eruptive volumes reconstructed where possible for the early flows that were subsequently buried.

Many vents can be tied to specific flows, with the exception of some of the early erupted units. For example, the vents of units bb4 and bb6 are within the interior of the Brushy Butte flow field and surrounded by later flows. These could be the vents for exposed flows that are not in contact as younger flows result in stranded cones, but this is difficult to determine based on similarities in geochemistry and paleomagnetism throughout the flow field. Two of the vent areas mapped as part of the flow field (units bb1 and bb2 on **Figure 3**) create topographic high areas along the southern margin of the flow field but both are stratigraphically below all other adjacent flows related to Brushy Butte. A sample from one of these vent areas (unit bb1) plots geochemically within the Brushy Butte flow field for all major-oxide and trace-element abundances. Access to the other vent system (unit bb2) is restricted, but its high-standing appearance and young-looking morphology suggest that it is also part of the flow field. Both units bb1 and bb2 are inferred to be vent systems for the earliest erupted part of the Brushy Butte flow field and any flows from them are suggested to be covered by younger flows.

Table 5 lists the range of geomorphic flow features present throughout the Brushy Butte flow field. These flows consist of both pāhoehoe (sometimes with inflated surfaces) and ʻaʻā with transitional flow types of slabby and rubbly pāhoehoe to platy ʻaʻā (**Figures 2C,D, 6A–D**). A number of the Brushy Butte units host poorly developed to well-established lava channels and levees (**Figures 6A–D**), some with channel breakouts (**Figure 6D**), leading to lava fans. Pressure ridges are a common geomorphic feature for some of the longer ʻaʻā flows (**Figure 6C**). Some units (bb8, bb11, bb13, bb14, and bb22) host lava ponds (**Figure 6B**).

TABLE 5 | Characteristics of the different vents and lava flows associated with eruption of the Brushy Butte flow field.

Pulse / Unit Name	Vent Type	Lava Flow Morphology	Maximum Flow Length (m)	Area (km^2)	Eruptive Volume (km^3)
Early(?)					
bb1	At least 6 scoria cones	No lava	0.0	0.82	0.01
bb2	5 small craters	Pāhoehoe and ʻaʻā	1.2	1.87	0.03
Pulse 1					
bb3	No vent	Dominantly pāhoehoe with minor ʻaʻā	12.0	140.07[a]	2.10
bb4	Scoria cone	No lava	0.0	0.04	0.00
bb5	Crater (300 × 200 m)	Poorly-developed channel, predominantly pāhoehoe	2.1	1.06[a]	0.02
bb6	Scoria cone	No lava	0.0	0.05	0.00
bb7	2 spatter cones	Poorly-developed channel and levees, predominantly pāhoehoe	1.2	0.36	0.01
bb8	Spatter cone	Channel, levees, lava pond, predominantly pāhoehoe	3.2	1.57[a]	0.02
bb9	Spatter cone	Channels, levees, channel breakouts, pressure ridges, pāhoehoe and ʻaʻā	2.2	1.13	0.02
bb10	2 spatter cones	Channels, levees, channel breakouts, pressure ridges, pāhoehoe and ʻaʻā	4.4	7.11	0.11
Pulse 2					
bb11	7 small craters	Channels, levees, channel breakouts, lava pond, pressure ridges, pāhoehoe and ʻaʻā	6.6	24.33	0.36
bb12	2 small craters	Channel, levees, pressure ridges, pāhoehoe and ʻaʻā	1.6	0.57	0.01
bb13	2 craters (315 × 250 m for the largest)	Channel, levees, perched lava pond, pressure ridges, pāhoehoe and ʻaʻā	7.6	7.95[a]	0.12
bb14	3 craters (110 × 90 m for the largest)	Channels, levees, channel breakouts, lava pond, pressure ridges, pāhoehoe and ʻaʻā	2.7	3.21	0.05
bb15	Spatter cone	Channel, levees, pressure ridges, pāhoehoe and ʻaʻā	3.2	1.19	0.02
bb16	Spatter cone	Poorly-developed channel, levees, predominantly ʻaʻā	4.73	2.81[a]	0.04
bb17	2 craters (50 × 50 m for the largest)	Channels, levees, channel breakouts, pāhoehoe and ʻaʻā	1.0	0.64	0.01
Pulse 3					
bb18	4 spatter cones	Channel, levees, channel breakouts, pressure ridges, pāhoehoe and ʻaʻā	7.6	18.27[a]	0.27
bb19	Spatter cone	Channel, levees, channel breakouts, pressure ridges, pāhoehoe and ʻaʻā	2.9	1.53	0.02
bb20	Spatter cone	Channel, levees, channel breakouts, pressure ridges, pāhoehoe and ʻaʻā	4.7	1.23[a]	0.02
bb21	Spatter cone	Poorly-developed channel and levees, pressure ridges, predominantly ʻaʻā	1.3	0.33	0.00
bb22	2 spatter cones	Channel, levees, channel breakouts, lava pond, pressure ridges, pāhoehoe and ʻaʻā	1.2	0.49	0.01
Pulse 4					
bb23	Spatter cone	Channels, levees, channel breakouts, pressure ridges, pāhoehoe and ʻaʻā	4.5	10.62	0.16
bb24	Spatter cone	Channel, levees, channel breakout, pressure ridges, pāhoehoe and ʻaʻā	1.9	1.26	0.02
bb25	Spatter cone	Channel, levees, pressure ridges, predominantly ʻaʻā, minor pāhoehoe	4.8	1.62	0.02
bb26	Spatter cone	Multiple channels, levees, pressure ridges, pāhoehoe and ʻaʻā	1.4	0.92	0.01
bb27	Spatter cone	Predominantly pāhoehoe	0.3	0.05	0.00
bb28	3 spatter cones and 1 crater (70 × 45 m)	Pressure ridges, predominantly pāhoehoe, minor ʻaʻā	0.6	0.33	0.01
bb29	Spatter cone	Predominantly pāhoehoe	0.3	0.09	0.00

[a]*Denotes areas that were reconstructed due to burial by later lava flows from the Brushy Butte flow field. Reconstructed areas represent the most conservative estimates of areas that were buried.*

The Brushy Butte flow field is unusual for a northern California tholeiitic basalt in that multiple vents and flows have constructed a high-standing edifice at ~150 m tall (**Figure 2B**). Tholeiitic basalts are generally tube fed and flow a long way (≥10 km) from their vent systems (e.g., Donnelly-Nolan et al., 1991; Kauahikaua et al., 1998; Clynne and Muffler, 2010). The only flow in the flow field with a tube is in unit bb13 and this tube is <1 km long and has collapsed creating skylights (**Figure 6B**). Typically flow distances (≥10 km) for tholeiitic basalts can be far enough that it is often hard to find the low-lying vent systems from which the lavas erupted. However, the Brushy Butte flow field has constructed an unusually tall edifice, and the flows, particularly for early erupted unit bb3, are located no more than ~10 km from their associated vent area.

We interpret the high-standing nature of the edifice of the interior of the Brushy Butte flow field to reflect the flat ground of the Fall

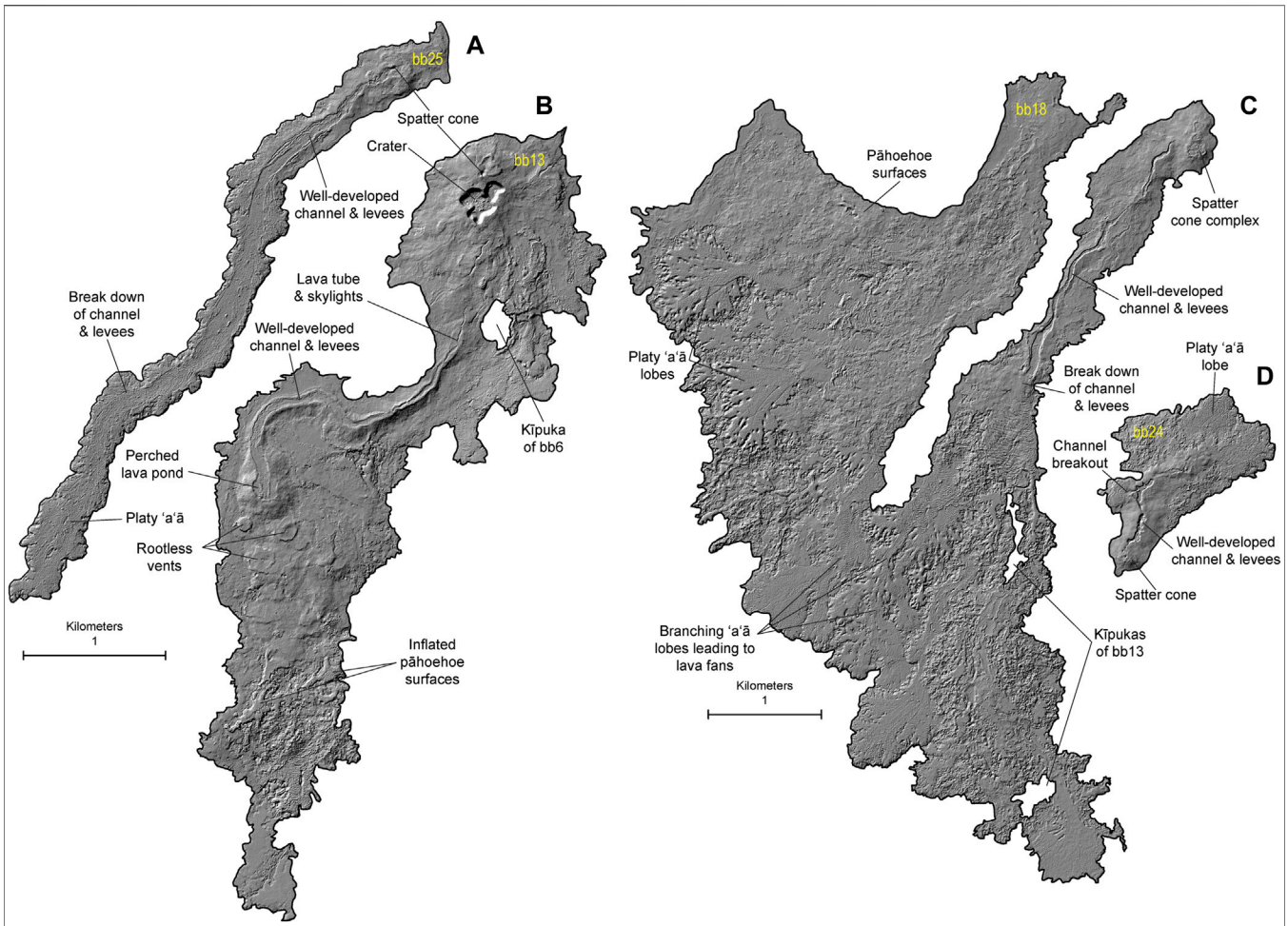

FIGURE 6 | 1 m-resolution lidar-derived hillshade showing the variety of volcanic landforms identified within the Brushy Butte flow field from units **(A)** bb25 **(B)** bb13 **(C)** bb18, and **(D)** bb24. These flow morphologies include well-established channels and levees of rubbly and slabby pāhoehoe and platy ‘a‘ā, breakouts through or over the top of levees, lava ponds, inflated pāhoehoe surfaces, spatter cones, and craters.

River Valley (**Figures 2A,B**). Eruption of lavas on flat ground allowed it to spread out in relatively equal proportions across the landscape, as well as hindering the development of tube systems that would result in flows several tens of kilometers long. The newly emplaced flows, while relatively flat themselves, would create their own topographic barriers and result in the roughly radial pattern around the vent systems in the interior of the flow field. As subsequent flows erupted from new vents within the interior, they took advantage of the new topography and flowed into low-lying areas, filling in the new topography and creating additional barriers within the interior of the flow field. As the eruptive period progressed, significantly reduced erupted volumes resulted in shorter flows. As a result, many of the younger flows were almost entirely confined to the interior of the flow field. The continuing emplacement process gradually constructed the high-standing interior edifice of the Brushy Butte flow field.

Eruptive Pulses

We arranged the units that make up the Brushy Butte flow field into stratigraphic order, where possible, using the 1 m-resolution lidar imagery and field studies. Based on this stratigraphic order and erupted volumes, we have defined pulses of eruptive activity from the flow field (**Figure 7**). Most Brushy Butte units group into four pulses. Pulse 1 consists of eight Brushy Butte units (bb3–bb10) and total 2.27 km^3 in eruptive volume, including the most voluminous (2.10 km^3) lava flow in unit bb3. The remaining units in pulse 1 are inferred to have erupted after bb3 based on their high-standing positions within the interior of the flow field, and each has a significantly smaller volume totalling only 0.27 km^3 for the other seven units of pulse 1 (**Table 5**). Pulse 2 consists of seven units (bb11–bb17) totalling 0.61 km^3 in eruptive volume, with the first unit (bb11) making up 0.36 km^3 of that total. Pulse 3 consists of five units (bb18–bb22) totalling 0.33 km^3 in eruptive volume, with the first unit (bb18) making up 0.27 km^3 of that total. Pulse 4 consists of seven units (bb23–bb29) totalling 0.22 km^3 in eruptive volume, with the first unit (bb23) making up 0.16 km^3 of that total.

The relative ages for pulses 2 and 3 are easy to reconstruct as there are ample places where direct contacts can be used to determine stratigraphic superposition. In pulses 1 and 4, however,

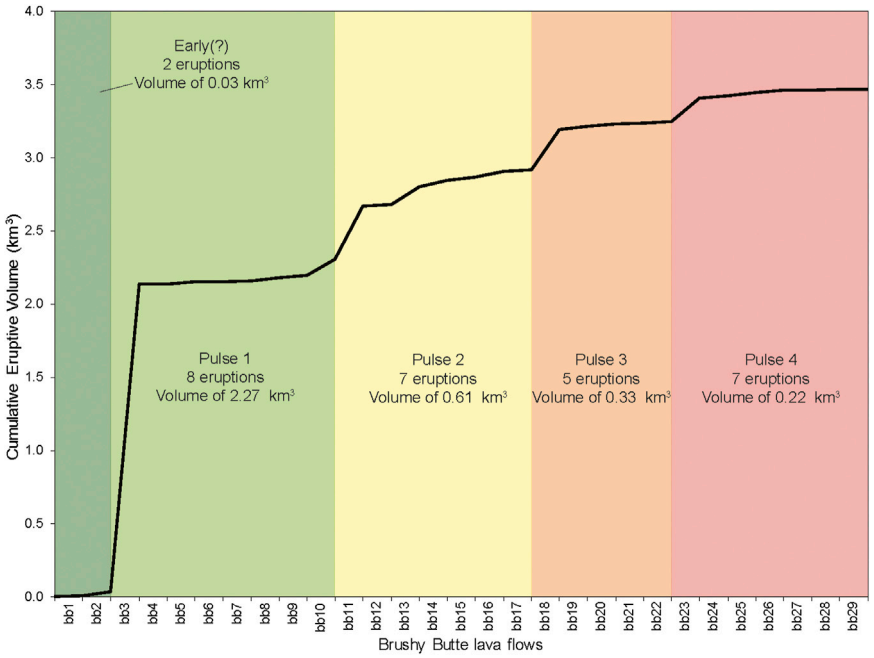

FIGURE 7 | Plot of cumulative eruptive volume (in km^3) for the Brushy Butte flow field (units bb1–bb29). The four distinct pulses based on stratigraphic order of flows and eruptive volume are highlighted by different colors.

flows are rarely in contact with each other. Therefore, the assigned unit number for flows from these pulses is somewhat arbitrary. For pulse 1, unit bb3 is easily inferred to underlie all flows erupted from the interior of the flow field based on its areal extent, despite its stratigraphic bracketing between units bb1 and bb10. This becomes more difficult for the rest of pulse 1, in which most units have no maximum relative age bracket because they are the oldest units exposed locally, with overlying bracketing units ranging anywhere from bb10 to bb23. Additionally, flows of pulse 1 are partly buried by younger flows from the flow field, with two vents (units bb4 and bb6) in the interior remaining uncorrelated with their flows. These vents could be the source(s) for exposed but disconnected flows, but no correlation can be made with the data on hand. As a result, we have mapped them as individual eruptive units attributed to the Brushy Butte flow field. On the other hand, units assigned to pulse 4 have no overlying units to bracket their relative ages, and none of these units are in direct contact. Underlying units can only constrain their relative ages to younger than bb13 (for bb28) or to younger than bb22 (for bb23). It is notable that map units bb25–bb29 in pulse 4 are relatively well aligned along the regional grain of normal faulting.

Brushy Butte units bb1 and bb2 have not been assigned to any pulse (they are labeled Brushy Butte early (?) on **Figure 3**), as it is unclear how these southern vent systems relate to the units erupted from the interior of the flow field. Only one sample from bb1 was collected for geochemistry, which is situated within the Brushy Butte geochemical field (**Figure 4**). The other early (?) erupted Brushy Butte map unit bb2 is densely faulted, but these faults only slightly extend into the overlying unit of bb11. This hints at bb2 being older than overlying Brushy Butte lavas, but not much older.

Despite these stratigraphic limitations, we can demonstrate, based on stratigraphic position, that the first eruption in each pulse 1–3 was the most voluminous, and we rely on this evidence to infer that the most voluminous eruption in pulse 4 (unit bb23) was also the first eruption of that pulse. All other flows assigned to pulse 4 were assigned a unit name arbitrarily, since they are not in direct contact. The erupted volumes of the other units in these pulses are too small to noticeably affect the volume distribution in **Figure 7**.

Just as each pulse shows an internal decay of eruptive volumes, each pulse itself shows a decrease in total eruptive volume from the previous pulse. Pulse 1 totals 2.27 km^3, which decreases to 0.61 km^3 for pulse 2, 0.33 km^3 for pulse 3, and 0.16 km^3 for pulse 4 (**Table 5**). This represents a decrease in eruptive volume of ~73% from pulse 1 to pulse 2, ~46% from pulse 2 to pulse 3, and ~32% from pulse 3 and pulse 4.

Eruption Duration

Despite no Holocene eruptions occurring outside of the major, long-lived volcanic centers of Mount Shasta, Medicine Lake Volcano, and the Lassen Volcanic Center (**Figure 1B**), volcanic activity between these centers is a distinct possibility. The lack of a witnessed northern California back-arc eruption makes it unclear how long such an eruption might last. Both field and laboratory evidence from the Brushy Butte flow field, when combined with analogue eruption styles, provide insights into the duration of such an eruption.

Some of the most extensively studied, first-hand accounts of tholeiitic basalt volcanism are from the East Rift Zone on the Island of Hawai'i, where Pu'u 'Ō'ō erupted continuously from 1983 to 2018. Over 35 years, the Pu'u 'Ō'ō eruption covered an area of ~144 km^2 and erupted a volume of ~4.4 km^3, while developing many geomorphic flow features (e.g., Hon et al., 1994; Kauahikaua et al., 1998; Hoblitt et al., 2012; Patrick and Orr, 2012). Volcanic landforms are constructed over a range of rates, providing clues as to the duration of eruptive activity in older volcanic terrains. For example, inflated pāhoehoe surfaces as high as 4 m have been observed forming in Hawai'i over the course of ~14 days (Hon et al., 1994; Hoblitt et al., 2012), a thickness similar to the 3–5 m inflated pāhoehoe from Brushy Butte. Unit bb3 has abundant inflated pāhoehoe surfaces, and we therefore propose that it took several weeks for the flow to be emplaced. The geomorphic features within the Brushy Butte flow field also suggest the possible duration of emplacement. These include well-established channel and levee systems with occasional breakouts and lava ponds (**Figures 6A–D**). Similar flow features in tholeiitic basalts of the Pu'u 'Ō'ō, as well as other Kīlauea eruptions, demonstrate that these sorts of features develop and last over the course of weeks, months, or longer (Patrick and Orr, 2012; Hazlett et al., 2019).

Paleomagnetic analysis provides further clues into the eruptive duration of the Brushy Butte flow field. In particular, pulses 1 and 3 both have mean remanent directions of magnetization that yield tight precision with small α95's. Pulse 1 encompasses 13 drill sites that yield a mean inclination of 60.9°, mean declination of 357.0°, and α95 of 1.0°. Pulse 3 yields a mean inclination of 58.8°, mean declination of 356.8°, and α95 of 1.6° from five drill sites (**Figure 5B**). While these two directions are very similar, an algorithm by McFadden and Jones (1981) indicates that they are distinct from each other at the 98% confidence level. Pulse 2 overlaps pulses 1 and 3 with a large α95 of 6.0° as a result of only two drill sites. This indicates that a very modest amount of time passed during these eruptions. For example, the immediately adjacent Giant Crater flow field is characterized by two distinct mean directions of remanent magnetization that are separated by 1.27° (from 58 drill sites) that has been modeled as an eruption spanning ~15 years based on rates of geomagnetic polar wander (Champion and Donnelly-Nolan, 1994). Our results give a probable eruptive duration for the Brushy Butte flow field (at least pulses 1–3) of 10–20 years, based on the average 4–5° per century of wander (Champion and Shoemaker, 1977).

CONCLUSION

Our investigation of the Brushy Butte flow field illustrates what eruptive styles and durations of tholeiitic basalt volcanism could occur in the Cascades back-arc of the western United States. A multidisciplinary approach to studying back-arc regions within the western United States demonstrate that these monogenetic tholeiitic basalts can erupt over decades from multiple, migrating vent systems. Their extents and large volumes spread out across the landscape, with the potential to impact populations and infrastructure. Investigations of past monogenetic, tholeiitic back-arc eruptions can provide clues into how a future eruption might progress, such as the eruption and emplacement of the Brushy Butte flow field.

The Brushy Butte flow field erupted at 35.7 ± 1.7 ka, constructing an edifice that is ~150 m tall, the longest flow lobes are >10 km long, and they cover an area of ~150 km^2 with an eruptive volume of at least 3.5 km^3. These flows were erupted from at least 28 vent areas consisting of scoria cones, spatter cones, and craters. The flows contain well-established channels and levees, channel breakouts, lava ponds, lava fans with pressure ridges, and inflated pāhoehoe surfaces. The eruptions can be divided into four pulses based on relative flow stratigraphy and volume. Pulse 1 is the most voluminous at 2.27 km^3 from eight eruptions; eruptive volumes decrease significantly to 0.61 km^3 for pulse 2, 0.33 km^3 for pulse 3, and 0.22 km^3 for pulse 4. Geochemical similarities between flow units of these pulses suggest that the eruption was continuous with little or no crustal storage time. The volcanic landforms within the Brushy Butte flow field indicate that individual units erupted over a duration of several weeks to months. Differences in mean remanent directions of magnetization (at least from pulses 1–3) show noticeable differences that do not overlap at the 98% confidence level, and are used to propose that the Brushy Butte flow field erupted over 10–20 years. This investigation documents the migrating eruptive vents and lava flows that could arise during a future monogenetic, tholeiitic basalt eruption in the western United States, with activity possibly occurring in pulses over the course of decades.

DATA AVAILABILITY STATEMENT

The original contributions presented in the study are included in the article/**Supplementary Material**, further inquiries can be directed to the corresponding author.

AUTHOR CONTRIBUTIONS

All authors undertook field mapping, stratigraphic studies, and participated in sample collection for analyses. DD and LM compiled the data into a map of the Brushy Butte flow field and surrounding flows. DD undertook sample preparation and analysis for the $^{40}Ar/^{39}Ar$ and ^{36}Cl dating. DC undertook sample preparation and analysis for paleomagnetism. MC undertook hand sample and thin section petrography to identify minerals from each flow and help distinguish differences between them. All authors contributed to interpretations and had a hand in writing the article.

FUNDING

This work was supported by the U.S. Geological Survey California Volcano Observatory.

ACKNOWLEDGMENTS

Thanks is owed to Peter Stent for access to his land during mapping and sample collecting. James Saburomaru, Dean Miller, Andrew Calvert, and Mark Stelten are thanked for help with the $^{40}Ar/^{39}Ar$ experiments. We appreciate the thoughtful reviews of Don Swanson, Aaron Pietruszka, Karoly Németh, Daniel Heaton, and the editorial handling of Rosa Anna Corsaro and Valerio Acocella, which greatly improved this paper. Any use of trade, firm, or product names is for descriptive purposes only, and does not imply endorsement by the United States government.

SUPPLEMENTARY MATERIAL

The Supplementary Material for this article can be found online at: https://www.frontiersin.org/articles/10.3389/feart.2021.639459/full#supplementary-material.

REFERENCES

Baker, M. B., Grove, T. L., Kinzler, R. J., Donnelly-Nolan, J. M., and Wandless, G. A. (1991). Origin of compositional zonation (high-alumina basalt to basaltic andesite) in the Giant Crater lava field, Medicine Lake volcano, northern California. *J. Geophys. Res.* 96, 21819–21842. doi:10.1029/91JB01945

Borg, L. E., Blichert-Toft, J., and Clynne, M. A. (2002). Ancient and modern subduction zone contributions to the mantle sources of lavas from the Lassen region of California inferred from Lu-Hf isotopic systematics. *J. Petrol.* 43, 705–723. doi:10.1093/petrology/43.4.705

Bromley, G. R. M., Thouret, J.-C., Schimmelpfennig, I., Mariño, J., Valdivia, D., Rademaker, K., et al. (2019). *In situ* cosmogenic ^{3}He and ^{36}Cl and radiocarbon dating of volcanic deposits refine the Pleistocene and Holocene eruption chronology of SW Peru. *Bull. Volcanol.* 81, 64. doi:10.1007/s00445-019-1325-6

Champion, D. E., and Donnelly-Nolan, J. M. (1994). Duration of eruption at the Giant Crater lava field, Medicine Lake volcano, California, based on paleomagnetic secular variation. *J. Geophys. Res.* 99, 15595–15604. doi:10.1029/94JB00900

Champion, D. E., Downs, D. T., Muffler, L. J. P., Clynne, M. A., and Calvert, A. T. (2017). "Geologic mapping of the Burney-Pit River area, California, using a multidisciplinary approach," in *International Association of Volcanology and Chemistry of the Earth's Interior*. Portland, Oregon, USA, Abstract VH13B-189, http://iavcei2017.org/IAVCEI%20 2017%20Abstracts.pdf.

Champion, D. E., and Shoemaker, E. M. (1977). Paleomagnetic evidence for episodic volcanism on the snake river plain. *NASA Tech. Memorandum* 78436, 7–9.

Christiansen, R. L., Calvert, A. T., and Grove, T. L. (2017). Geologic field-trip guide to Mount Shasta volcano, northern California. *U.S. Geol. Surv. Sci. Inv. Rep.* 2017-5022-K3, 1–34. doi:10.3133/sir20175022K3

Christiansen, R. L., Clynne, M. A., and Muffler, L. J. P. (2002). Geologic map of the Lassen Peak, Chaos Crags, and upper Hat Creek area, California. *U.S. Geol. Surv. Geol. Inv. Ser.* I-2733, 1–17. scale 1:24,000.

Clynne, M. A., Calvert, A. T., Champion, D. E., Muffler, L. J. P., Sawlan, M. G., and Downs, D. T. (2017). Age of the youngest volcanism at Eagle Lake, northeastern California-$^{40}Ar/^{39}Ar$ and paleomagnetic results. *U.S. Geol. Surv. Open-file Rep.* 2017–1027, 1–24. doi:10.3133/ofr20171027

Clynne, M. A., and Muffler, L. J. P. (2017). Geologic field-trip guide to the Lassen segment of the Cascades arc, northern California. *U.S. Geol. Surv. Sci. Inv. Rep.* 2017-5022-K2, 1–65. doi:10.3133/sir20175022K2

Clynne, M. A., and Muffler, L. J. P. (2010). Geologic map of Lassen Volcanic National Park and vicinity, California. *U.S. Geol. Surv. Sci. Inv. Map* 2899, 1–110. scale 1:50,000, 3 sheets.

Conrey, R. M., Bailey, D. G., Singer, J. W., Wagoner, L., Parfitt, B., Hay, J., et al. (2019). Optimization of internal standards in LA-ICP-MS analysis of geologic samples using lithium borate fused glass. *Geol. Soc. Am. Abs.* 51. doi:10.1130/abs/2019NE-328672

Donnelly-Nolan, J. M., Champion, D. E., Grove, T. L., Baker, M. B., Taggart, J. E., Jr., and Bruggman, P. E. (1991). The Giant Crater lava field: geology and geochemistry of a compositionally zoned, high-alumina basalt to basaltic andesite eruption at Medicine Lake Volcano, California. *J. Geophys. Res.* 96, 21843–21863. doi:10.1029/91JB01901

Donnelly-Nolan, J. M., Champion, D. E., and Grove, T. L. (2016). Late Holocene volcanism at Medicine Lake volcano, northern California Cascades. *U.S. Geol. Surv. Prof. Pap.* 1822, 1–59. doi:10.3133/pp1822

Donnelly-Nolan, J. M. (2010). Geologic map of Medicine Lake volcano, northern California. *U.S. Geol. Surv. Sci. Inv. Map* 2927, 1–48. doi:10.3133/sim2927

Donnelly-Nolan, J. M., and Grove, T. L. (2017). Geologic field-trip guide to Medicine Lake volcano, northern California, including Lava Beds National Monument. *U.S. Geol. Surv. Sci. Inv. Rep.* 2017–5022–K1, 1–53. doi:10.3133/sir20175022K1

Downs, D. T., Champion, D. E., Muffler, P., Christiansen, R. L., Clynne, M. A., and Calvert, A. T. (2020a). Simultaneous Middle Pleistocene eruption of three widespread tholeiitic basalts in northern California (USA): insights into crustal magma transport in an actively extending back arc. *Geology* 48, 1216–1220. doi:10.1130/G48076.1

Downs, D. T., Clynne, M. A., Champion, D. E., and Muffler, L. J. P. (2020b). Eruption age and duration of the ~9 km^3 Burney Mountain dacite dome complex, northern California, USA. *Geol. Soc. Am. Bull.* 132, 1150–1164. doi:10.1130/B35240.1

Downs, D. T., Robinson, J. E., Stelten, M. E., Champion, D. E., Dietterich, H. R., Sisson, T. W., et al. (2019). Geologic map of the northern Harrat Rahat volcanic field, Kingdom of Saudi Arabia. *U.S. Geol. Surv. Sci. Inv. Map* 3428, 1–65. 4 sheets, scales 1:75,000, 1:25,000. doi:10.3133/sim3428

Downs, D. T., Stelten, M. E., Champion, D. E., Dietterich, H. R., Nawab, Z., Zahran, H., et al. (2018). Volcanic history of the northernmost part of the Harrat Rahat volcanic field, Saudi Arabia. *Geosphere* 14, 1253–1282. doi:10.1130/GES01625.1

Ewert, J. W., Diefenbach, A. K., and Ramsey, D. W. (2018). 2018 update to the U.S. Geological Survey national volcanic threat assessment. *U.S. Geol. Surv. Sci. Inv. Rep*, 2018–5140. 1–40. doi:10.3133/sir20185140

Ewert, J. W., Guffanti, M. C., and Murray, T. L. (2005). An assessment of volcanic threat and monitoring capabilities in the United States—Framework for a National Volcano Early Warning System. *U.S. Geol. Surv. Open-File Rep.* 2005-1164, 1–62.

Ewert, J. W. (2007). System for ranking relative threats of U.S. Volcanoes. *Nat. Hazards Rev.* 8, 112–124. doi:10.1061/(asce)1527-6988(2007)8:4(112)

Fleck, R. J., Calvert, A. T., Coble, M. A., Wooden, J. L., Hodges, K., Hayden, L. A., et al. (2019). Characterization of the rhyolite of Bodie Hills and $^{40}Ar/^{39}Ar$ intercalibration with Ar mineral standards. *Chem. Geology.* 525, 282–302. doi:10.1016/j.chemgeo.2019.07.022

Grose, T. L. T. (1999). Geologic map of the Fall River Mills 15' quadrangle, Lassen, Modoc, and Siskiyou counties, California. *California Division of Mines and Geology*, scale 1:62,500.

Guffanti, M., Clynne, M. A., Smith, J. G., Muffler, L. J. P., and Bullen, T. D. (1990). Late Cenozoic volcanism, subduction, and extension in the Lassen region of California, southern Cascade range. *J. Geophys. Res.* 95, 19453–19464. doi:10.1029/JB095iB12p19453

Hazlett, R. W., Orr, T. R., and Lundblad, S. P. (2019). Undocumented late 18th- to early 19th-century volcanic eruptions in the Southwest Rift Zone of Kīlauea volcano, Hawai'i. *U.S. Geol. Surv. Sci. Inv. Rep.* 5010, 1–13. doi:10.3133/sir20195010

Hildreth, W. (2007). Quaternary magmatism in the Cascades—geologic perspectives. *U.S. Geol. Surv. Prof. Pap.* 1744, 1–125.

Hoblitt, R., Orr, T. R., Heliker, C., Denlinger, R. P., Hon, K., and Cervelli, P. F. (2012). Inflation rates, rifts, and bands in a pāhoehoe sheet flow. *Geosphere* 8, 179–195. doi:10.1130/GES00656.1

Hon, K., Kauahikaua, J., Denlinger, R., and Mackay, K. (1994). Emplacement and inflation of pahoehoe sheet flows: observations and measurements of active lava flows on Kilauea Volcano, Hawaii. *Geol. Soc. Am. Bull.* 106, 351–370. doi:10.1130/0016-7606(1994)106<0351:eaiops>2.3.co;2

Irwin, W. P. (2003). Correlation of the Klamath mountains and Sierra Nevada. *U.S. Geol. Surv. Open-file Rep.* 02-490, 2 sheets.

Johnson, D. M., Hooper, P. R., and Conrey, R. M. (1999). XRF analysis of rocks and minerals for major and trace elements on a single low dilution Li-tetraborate fused bead. *JCPDS-International Centre for Diffraction Data*, 843–867.

Kauahikaua, J., Cashman, K. V., Mattox, T. N., Heliker, C. C., Hon, K. A., Mangan, M. T., et al. (1998). Observations on basaltic lava streams in tubes from Kilauea Volcano, Island of Hawai'i. *J. Geophys. Res.* 103, 27303–27323. doi:10.1029/97JB03576

Lee, J.-Y., Marti, K., Severinghaus, J. P., Kawamura, K., Yoo, H.-S., Lee, J. B., et al. (2006). A redetermination of the isotopic abundances of atmospheric Ar. *Geochimica et Cosmochimica Acta* 70, 4507–4512. doi:10.1016/j.gca.2006.06.1563

Lifton, N., Sato, T., and Dunai, T. J. (2014). Scaling *in situ* cosmogenic nuclide production rates using analytical approximations to atmospheric cosmic-ray fluxes. *Earth Planet. Sci. Lett.* 386, 149–160. doi:10.1016/j.epsl.2013.10.052

Machette, M., Haller, K., and Wald, L. (2004). Quaternary fault and fold database for the nation. *U.S. Geol. Surv. Fact Sheet* 2004-3033.

Marrero, S. M., Phillips, F. M., Borchers, B., Lifton, N., Aumer, R., and Balco, G. (2016). Cosmogenic nuclide systematics and the CRONUScalc program. *Quat. Geochronol.* 31, 160–187. doi:10.1016/j.quageo.2015.09.005

McElhinny, M. W. (1973). *Paleomagnetism and plate tectonics*. Cambridge, United Kingdom: University Press.

McFadden, P. L., and Jones, D. L. (1981). The fold test in palaeomagnetism. *Geophys. J. Int.* 67, 53–58. doi:10.1111/j.1365-246X.1981.tb02731.x

Miller, C. D. (1989). Potential hazards from future volcanic eruptions in California. *U.S. Geol. Surv. Bull.* 1847, 1–17.

Muffler, L. J. P., Calvert, A. T., Champion, D. E., Clynne, M. A., Downs, D. T., and Christiansen, R. L. (2017). "The Cascades volcanic arc between the Lassen Volcanic Center and Mount Shasta, northern California," in *International Association of Volcanology and Chemistry of the Earth's Interior*. Portland, Oregon, USA, Abstract VH13B-190, http://iavcei2017. org/IAVCEI%202017%20Abstracts.pdf.

Muffler, L. J. P., Clynne, M. A., and Champion, D. E. (1994). Late Quaternary normal faulting of Hat Creek Basalt, northern California. *Geol. Soc. Am. Bull.* 106, 195–200. doi:10.1130/0016-7606(1994)106<0195:LQNFOT>2.3.CO;2

Muffler, L. J. P., and Clynne, M. A. (2015). Geologic field-trip guide to Lassen Volcanic National Park and vicinity, California. *U.S. Geol. Surv. Sci. Inv. Rep.* 2015-5067, 1–67. doi:10.3133/sir20155067

Németh, K., and Kereszturi, G. (2015). Monogenetic volcanism: personal views and discussion. *Int. J. Earth Sci. (Geol Rundsch)* 104, 2131–2146. doi:10.1007/s00531-015-2143-6

Patrick, M. R., and Orr, T. R. (2012). Rootless shield and perched lava pond collapses at Kīlauea Volcano, Hawai'i. *Bull. Volcanol.* 74, 67–78. doi:10.1007/s00445-011-0505-9

Peterson, J. A., and Martin, L. M. (1980). Geologic map of the Baker -Cypress BLM roadless area and Timbered Crater Rare II areas, Modoc, Shasta, and Siskiyou counties, California. *U.S. Geol. Surv. Misc. Field Stud*. Map MF -1214 -A, scale 1: 62,500. doi:10.3133/mf1214A

Steiger, R. H., and Jäger, E. (1977). Subcommission on geochronology: convention on the use of decay constants in geo- and cosmochronology. *Earth Planet. Sci. Lett.* 36, 359–362. doi:10.1016/0012-821X(77)90060-7

Stelten, M. E., Downs, D. T., Champion, D. E., Dietterich, H. R., Calvert, A. T., Sisson, T. W., et al. (2020). The timing and compositional evolution of volcanism within northern Harrat Rahat, Kingdom of Saudi Arabia. *Geol. Soc. Am. Bull.* 132, 1381–1403. doi:10.1130/B35337.1

Stelten, M. E., Downs, D. T., Dietterich, H. R., Mahood, G. A., Calvert, A. T., Sisson, T. W., et al. (2018). Timescales of magmatic differentiation from alkali basalt to trachyte within the Harrat Rahat volcanic field, Kingdom of Saudi Arabia. *Contrib. Mineral. Petrol.* 173, 68. doi:10.1007/s00410-018-1495-9

Taggart, J. E., Jr. (2002). Analytical methods for chemical analysis of geologic and other materials, U.S. Geological Survey. *U.S. Geol. Surv. Open-File Rep.*, 02–223. 1–20. doi:10.3133/ofr02223

Turrin, B. D., Muffler, L. J. P., Clynne, M. A., and Champion, D. E. (2007). Robust 24±6 ka $^{40}Ar/^{39}Ar$ age of a low-potassium tholeiitic basalt in the Lassen region of NE California. *Quat. Res.* 68, 96–110. doi:10.1016/j.yqres.2007.02.004

Vazquez, J. A., and Woolford, J. M. (2015). Late Pleistocene ages for the most recent volcanism and glacial-pluvial deposits at Big Pine volcanic field, California, USA, from cosmogenic ^{36}Cl dating. *Geochem. Geophys. Geosyst.* 16, 2812–2828. doi:10.1002/2015GC005889

Walker, G. P. L. (1973). Lengths of lava flows. *Phil. Trans. R. Soc. A*. 274, 107–118. doi:10.1098/rsta.1973.0030

Wood, C. A. (1979). Monogenetic volcanoes of the terrestrial planets. *Proc. 10th Lunar Planet. Sci. Conf*. New York, Pergamon Press, 2815–2840. Available at: http://articles.adsabs.harvard.edu/pdf/1979LPSC...10.2815W.

Conflict of Interest: The authors declare that the research was conducted in the absence of any commercial or financial relationships that could be construed as a potential conflict of interest.